# Medical Physics and Engineering Days

February 13 – 14, 2025, Tampere, Finland

Program and Abstract Book

Milla Juutinen and Jari Viik (eds.)

Lääketieteellisen fysiikan ja tekniikan yhdistys (LFTY)
Finnish Society for Medical Physics and Medical Engineering

# LFT-päivät Tampereella 13.-14.2.2025

Medical Physics and Medical Engineering Days in Tampere 2025

| Table of contents: | Page |
|---|---|


*Thank you for official supporters and sponsors of the Medical Physics and Medical Engineering Days*

# LFT Days Program

*The Finnish Society for Medical Physics and Medical Engineering organizes an annual event for students, researchers and companies in our field, Medical Physics and Engineering (LFT) Days. In 2025, the event will be held in Tampere on February 13-14 in auditorium TB104 on Tietotalo building (Korkeakoulunkatu 1, 33720 Tampere).*

Day 1: Examples of LFT Research in Tampere, Company Presentations and MSc Poster Competition
Day 2: Presentations on PhD research projects

## Day 1: Thursday 13.2.2025, Tietotalo

08:30 Coffee, Registration, Posters setup

**09:00 Opening by the Chair of LFT Society – Simo Särkkä**
**09:05 Greetings from the Dean – Seppo Parkkila**
**09:10 Local event information – Jari Viik**

**09:15 Selected Health Tech Research at Tampere University** (chair Leena Ukkonen)
09:15 Research in Biomedical Technology (TECH) Unit, Prof. Leena Ukkonen
09:40 Integration of in-vitro, in-silico and Data-based Models for Personalized Digital Twin Solution - Case HCM, Prof. Jari Hyttinen
09:55 Center of Excellence in Body-on-Chip Research, Prof. Minna Kellomäki
10:10 Vascularized Organ-on-a-Chip Models, PostDoc Fellow Hanna Vuorenpää
10:25 Health Data Science, Prof. Matti Nykter
10:40 Medical Physics Research Projects in Tays
Medical Imaging, Associate Chief Physicist Kirsi Holli-Helenius
Clinical Neurophysiology, Associate Chief Physicist Mirja Tenhunen

11:00 Break (15 min), Sponsor stands

**11:15 Poster Competition: 3 min Power Pitch + traditional posters** (chair Jari Hyttinen)
11:15 Karim Ameziane, *A Hypoxia-Maintaining Perfusion Device for Prolonged Cell Studies*
11:20 Praveen Dedigamage, *A Spiking Neural Network Based Pipeline for Motor Imagery EEG Classification*
11:25 Mohsen Haajari, *Portable Olfactory Display for Healthcare Applications*
11:30 Hiran Maladenige, *Objective Radiotherapy Treatment Plan Evaluation Tool to Support Planning Automation*
11:35 Inka Mustajoki, *Detection of Infectious Respiratory Diseases Using Wearable Devices*
11:40 Lotta Mäkinen, *The Effect of ALD Coating Composition on Coating Adhesion and In Vitro Degradation of Orthopedic Magnesium Alloy Implants*
11:45 Ilona Mäkinen, *Computational Modelling of Energy Metabolism in Schizophrenia*
11:50 Jutta Nurminen, *Determining the Circulatory Responses Related to Respiratory Events from the Photoplethysmography Signal*
11:55 Samuel Onnela, *Signal-To-Equivalent Thickness Calibration (STC) - Menetelmä parantaa pehmyskudoskontrastia kliinisessä KKTT-kuvantamisessa*
12:00 Karoliina Puronhaara, *Utilising Fourier Neural Operators for Ultrasound Field Simulation in Photoacoustic Tomography*
12:05 Kati Rinnekari, *Hydrogel Screening for 3D Vascular Model on Microfluidic Chip*
12:10 Markus Tolvanen, *Fabrication and Characterization of Optical-Resolution Photoacoustic Microscope*

12:15 Miika Vainikka, *Quantifying and Analyzing Uncertainty in Automatic Sleep Staging with Neural Networks*
12:20 Sofia Voimanen, *Not Too Harmful, Not Too Still but Just Right: Characteristics of an Ultrasonic Toothbrush*
12:25 Lassi Vuononvirta, *Changes in Joint Space Width After Drastic Weight Loss*
12:30 Kaisla Walls, *The effect of Levosimendan Metabolite OR-1896 on Ischemic Human-Induced Pluripotent Stem Cell-Derived Cardiomyocytes: Studying Arrhythmias During Acute Hypoxia*

12:40 Lunch (at own cost), Sponsor stands, Socializing & Posters meeting

**14:00 Company Presentations** (chair Jani Keyriläinen)
14:00 Siemens Healthcare, Marko Pesola
14:15 Radicare, Wenze van Klink
14:30 Brainlab, Jesse Paavola
14:45 MVision AI, Jani Pehkonen

15:00 Coffee break (30 min), Sponsor stands, Socializing & Poster meeting

**15:30 Company Presentations continue** (chair Jari Viik)
15:30 Mirion Technologies, Jan-Patrik Libäck
15:45 Vision RT, Jonathan Rosser and Katja Lanu
16:00 Nexstim

**16:15 Results of Poster Competition, Awards, Closing of the day, Simo Särkkä and Jari Viik**

**17:00 Evening Gathering – Ravintola Orvokki, Hermiankatu 6–8, 33720 Tampere**

Navigation instructions for walking to the restaurant, (Google Maps route)
https://maps.app.goo.gl/9iCMsHzFeoETR3oA8

The most straight-forward route to restaurant Orvokki is by walking Hervannan Valtaväylä until Hermiankatu (~ 400 m in total).

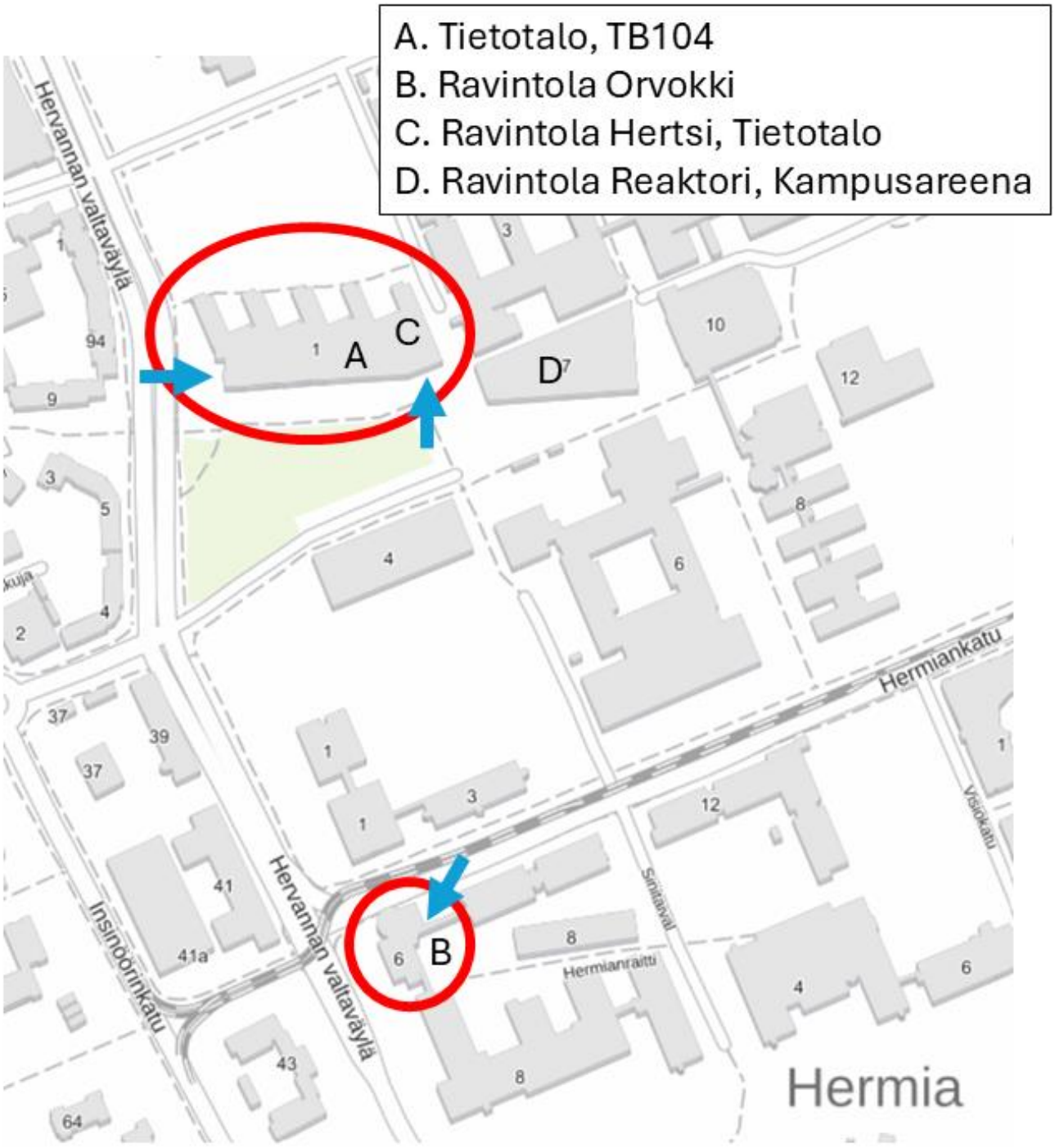
A. Tietotalo, TB104
B. Ravintola Orvokki
C. Ravintola Hertsi, Tietotalo
D. Ravintola Reaktori, Kampusareena
A
B
C
D
Hervannan valtaväylä
Hermiankatu
Insinöörinkatu
Hermianraitti
Visiokatu
Hermia

## Day 2: Friday 14.2.2025, Tietotalo

08:00 Coffee, Registration, PhD posters setup

**08:15 Opening by Local Organizers & LFT Best Paper 2024 Award Introduction**

**08:20 LFT Best Paper 2024 Award Presentation** (chair Simo Särkkä)
8:20 Tuomo Mäki-Marttunen, *Genetic Mechanisms for Impaired Synaptic Plasticity in Schizophrenia Revealed by Computational Modeling*
8:32 Antti Kiviaho, *Single Cell and Spatial Transcriptomics Highlight the Interaction of Club-Like Cells with Immunosuppressive Myeloid Cells in Prostate Cancer*

**08:45 Presentation Session 1** (chair Antti Ahola)
8:45 Elois Canals, *Predicting Cartilage Thickness Maps from Multispectral Imaging using Deep Learning*
8:56 Atte Joutsen, *Dry Electrode Solutions for Measuring Cardiac Activity in Wearable Technology*
9:07 Seyed Mahan Nematollahi Sanij, *Estimating Knee Joint Cartilage Mechanics Using Finite Element by Neural Network Based Kinetic Data*
9:18 Laura Keto, *Deciphering Cerebellar Astroglial Calcium Dynamics with Detailed Whole-Cell Modeling*

09:30 Break (60 min), Sponsor stands, Socializing & PhD poster meeting

**09:30 Annual Meeting of the LFT Society, room TC103**

**10:30 Presentation Session 2** (chair Miina Björninen)
10:30 Akuroma George, *Diffuse Reflectance Spectroscopy for Characterization of Tissue Optical Properties*
10:41 Sonya Ghanavati, *Biophotonic Composite Scaffolds for Controlled Nitric Oxide Release Upon NIR Excitation*
10:52 Virginia Alessandra Gobbo, *Impact of Protein Adsorption on Bioactive Glasses and Biological Response: A Step Forward Towards a Predictable Cell Fate*
11:03 Harina Karunarathna, *Adaptation of Near Infrared Spectroscopy for In Situ Monitoring of Tissue Engineered Cartilage Growth*
11:14 Nithin Sadeesh, *Investigating the Effects of Inflammatory Factors on Joint Tissues Using Near-Infrared (NIR) Spectroscopy on Explant Culture Medium*

11:25 Lunch (at own cost), Sponsor stands, Socializing & PhD poster meeting

**12:15 Presentation session 3** (chair Emre Kapucu)
12:15 Kaisa Tornberg, *Combining Microfluidic Technology with Human Based Cell Models to Build Body-On-Chip for Stroke-Heart Syndrome*
12:26 Katja Törmä, *Multivariate Directed Functional Connectivity Methods for Estimation of Whole-Brain Connectivity*
12:37 Saana Seppälä, *Impaired Memory Storage and Recall of Hippocampal CA1-CA3 Network In Early Alzheimer's Disease*
12:48 Uzman Ali, *Implant-To-Implant Communications Using Quad-Band Pifas for Intracranial Applications*

**13:00 Closing of LFT Days, Simo Särkkä and Jari Viik**

*Trains to Helsinki 14:00, Kuopio 14:07, Oulu 14:02 and Turku 14:10.*

# Finnish Society for Medical Physics and Medical Engineering Best Paper 2024 Award

## 1st place, shared

**Single Cell and Spatial Transcriptomics Highlight the Interaction of Club-Like Cells with Immunosuppressive Myeloid Cells in Prostate Cancer**

**Antti Kiviaho**, Sini K. Eerola, Heini M. L. Kallio, Maria K. Andersen, Miina Hoikka, Aliisa M. Tiihonen, Iida Salonen, Xander Spotbeen, Alexander Giesen, Charles T. A. Parker, Sinja Taavitsainen, Olli Hantula, Mikael Marttinen, Ismaïl Hermelo, Mazlina Ismail, Elise Midtbust, Maximilian Wess, Wout Devlies, Abhibhav Sharma, Sebastian Krossa, Tomi Häkkinen, Ebrahim Afyounian, Katy Vandereyken, Sam Kint, Juha Kesseli, Teemu Tolonen, Teuvo L. J. Tammela, Trond Viset, Øystein Størkersen, Guro F. Giskeødegård, Morten B. Rye, Teemu Murtola, Andrew Erickson, Leena Latonen, G. Steven Bova, Ian G. Mills, Steven Joniau, Johannes V. Swinnen, Thierry Voet, Tuomas Mirtti, Gerhardt Attard, Frank Claessens, Tapio Visakorpi, Kirsi J. Rautajoki, May-Britt Tessem, Alfonso Urbanucci, and Matti Nykter

*Nature Communications 2024 Nov 16;15(1):9949.*

**Genetic Mechanisms for Impaired Synaptic Plasticity in Schizophrenia Revealed by Computational Modeling**

**Tuomo Mäki-Marttunen**, Kim T. Blackwell, Ibrahim Akkouh, Alexey Shadrin, Mathias Valstad, Torbjørn Elvsåshagen, Marja-Leena Linne, Srdjan Djurovic, Gaute T. Einevoll, and Ole A. Andreassen

*Proceedings of the National Academy of Sciences of the United States of America 2024 Aug 20;121(34):e2312511121.*

# MSc Thesis Poster Competition

1. **KARIM AMEZIANE**, A HYPOXIA-MAINTAINING PERFUSION DEVICE FOR PROLONGED CELL STUDIES

2. **PRAVEEN DEDIGAMAGE**, A SPIKING NEURAL NETWORK BASED PIPELINE FOR MOTOR IMAGERY EEG CLASSIFICATION

3. **MOHSEN HAAJARI**, PORTABLE OLFACTORY DISPLAY FOR HEALTHCARE APPLICATIONS

4. **HIRAN MALADENIGE**, OBJECTIVE RADIOTHERAPY TREATMENT PLAN EVALUATION TOOL TO SUPPORT PLANNING AUTOMATION

5. **INKA MUSTAJOKI**, DETECTION OF INFECTIOUS RESPIRATORY DISEASES USING WEARABLE DEVICES

6. **LOTTA MÄKINEN**, THE EFFECT OF ALD COATING COMPOSITION ON COATING ADHESION AND IN VITRO DEGRADATION OF ORTHOPEDIC MAGNESIUM ALLOY IMPLANTS

7. **ILONA MÄKINEN**, COMPUTATIONAL MODELLING OF ENERGY METABOLISM IN SCHIZOPHRENIA

8. **JUTTA NURMINEN**, DETERMINING THE CIRCULATORY RESPONSES RELATED TO RESPIRATORY EVENTS FROM THE PHOTOPLETHYSMOGRAPHY SIGNAL

9. **SAMUEL ONNELA**, SIGNAL-TO-EQUIVALENT THICKNESS CALIBRATION (STC) - MENETELMÄ PARANTAA PEHMYSKUDOSKONTRASTIA KLIINISESSÄ KKTT-KUVANTAMISESSA

10. **KAROLIINA PURONHAARA**, UTILISING FOURIER NEURAL OPERATORS FOR ULTRASOUND FIELD SIMULATION IN PHOTOACOUSTIC TOMOGRAPHY

11. **KATI RINNEKARI**, HYDROGEL SCREENING FOR 3D VASCULAR MODEL ON MICROFLUIDIC CHIP

12. **MARKUS TOLVANEN**, FABRICATION AND CHARACTERIZATION OF OPTICAL-RESOLUTION PHOTOACOUSTIC MICROSCOPE

13. **MIIKA VAINIKKA**, QUANTIFYING AND ANALYZING UNCERTAINTY IN AUTOMATIC SLEEP STAGING WITH NEURAL NETWORKS

14. **SOFIA VOIMANEN**, NOT TOO HARMFUL, NOT TOO STILL BUT JUST RIGHT: CHARACTERISTICS OF AN ULTRASONIC TOOTHBRUSH

15. **LASSI VUONONVIRTA**, CHANGES IN JOINT SPACE WIDTH AFTER DRASTIC WEIGHT LOSS

16. **KAISLA WALLS**, THE EFFECT OF LEVOSIMENDAN METABOLITE OR-1896 ON ISCHEMIC HUMAN-INDUCED PLURIPOTENT STEM CELL-DERIVED CARDIOMYOCYTES: STUDYING ARRHYTHMIAS DURING ACUTE HYPOXIA

# A HYPOXIA-MAINTAINING PERFUSION DEVICE FOR PROLONGED CELL STUDIES

**Karim Ameziane (1), Joose Kreutzer (1), Hannu Välimäki (1), Veikko Sariola (2), Pasi Kallio (1)**

1. *Faculty of Medicine and Health Technology, Micro- and Nanosystems Group, Tampere University, Finland*
2. *Faculty of Medicine and Health Technology, Bioinspired Materials and Robotics Group, Tampere University, Finland*

## Introduction

Although oxygen accounts for 21% of the air's composition around us, our organs generally harbour much lower oxygen concentrations [1]. Despite the importance of oxygen in the replication of physiological conditions, it typically remains unaccounted for in cell studies [2][3]. The device presented in this study could bring cell cultures closer to *in vivo* conditions to better replicate and understand the behaviour of tissues in their physiological environment.

## Methods

The device consists of a medium channel surrounded by a gas channel, separated by an oxygen permeable wall. These channels are cast as a single piece from polydimethylsiloxane (PDMS) using a 3D-printed mould. A laser-cut barrier preventing oxygen diffusion from ambient air is then placed on top of the device and the channels are sealed onto a microscope slide.

The device's behaviour is characterized by measuring the step response to changes in oxygen tension under various flow rates. These measurements are performed optically under a microscope using a ratiometric sensor layer. Additionally, a finite element method (FEM) simulation model is developed to replicate the device's behaviour *in silico*.

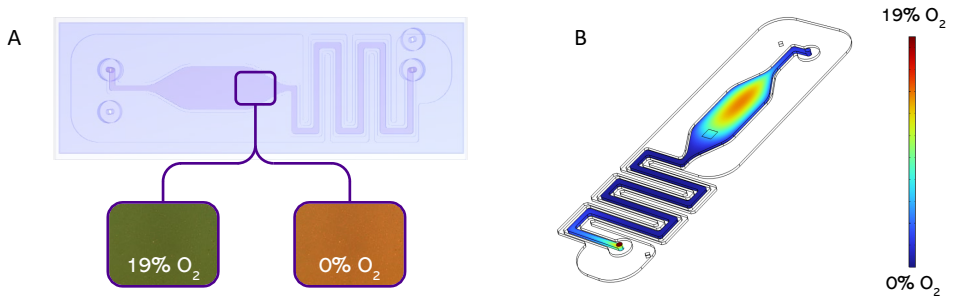


*Figure 1: The hypoxia-maintaining perfusion device. A) The ratiometric sensor layer reacts to the oxygen tension in the measured area. B) The simulation model replicates the measured data and predicts the device's behaviour in other regions under various conditions.*

## Results

With a flow rate of 4 µL/min, the device can set hypoxic conditions in 52 min. The device can also maintain set oxygen conditions with flow rates below 10 µL/min. Additionally, the simulation model can replicate the measured behaviour under different conditions. According to the model, the device is estimated to set hypoxic conditions in 27 min at the 10 µL/min flow rate limit.

## Discussion

The presented device is capable of successfully combining simultaneous oxygen control and perfusion of the medium channel. Moreover, the developed FEM model mirrors the measurements and offers insight on the device's behaviour outside the measured area. This device could be used in studies involving cell cultures to better study their behaviour under both hypoxia and normoxia.

## References

1. Brennan M.D. et al., Lab Chip, 14:4305–18, 2014.
2. Place T.L. et al., Free Radical Biology and Medicine, 113:311–22, 2017.
3. Mas-Bargues C. et al., IJMS, 20:1195, 2019.

# MINIATURISED OLFACTORY DISPLAY

**Mohsen Haajari (1,2)*, Timo Salpavaara (1), Jussi Rantala (2), Pasi Kallio (1), Veikko Surakka (2)**

*1. Micro and Nano systems Research Group, Tampere University, FINLAND;*
*2. Emotions, Sociality, and Computing Research Group, Tampere University, FINLAND*

## Introduction

Human sense of smell is the oldest but still least studied of all our senses. Olfactory displays (OD) are devices that are used to stimulate the human sense of smell [1]. The integration of olfactory stimuli in digital and virtual environments remains limited by hardware challenges such as weight and size, response time, number of inlet odors, and contamination [2].
This thesis presented a concept of olfactory display based on digital microfluidics (DMF). DMF is a technique for manipulating microliter droplets in virtual and programmable fluidic channels. The thesis aim was proof of concept by answering these research questions: (1) Is it feasible to use digital microfluidics for designing olfactory displays? (2) What are the potentials and limitations of digital microfluidics in this context?

## Methods

The thesis includes hardware and software development and technical and human tests. As the fabrication of a DMF module is outside the thesis' scope, commercial modules were used to check the idea's feasibility and explore limitations and opportunities for future development. A desktop olfactory display was developed, including a commercial DMF module, a micropump, a piezoelectric evaporator, and a controller board.

## Results

The device was tested using food-grade liquid odors such as rose, mint, and chicory water. Functions such as sampling and delivering odor droplets were analyzed by video frame analysis to explore the potential and limitations of DMF in the OD context. The scented air was analyzed by photoionization detector (PID), and it showed these odors have weak PID signals in comparison with isopropyl alcohol (IPA). The assessed response time in the PID detector was 11 seconds. In the human study, participants were randomly exposed to three droplets of three different odors (rose, mint, and chicory water), and the task was to identify each odor through the developed software. The ratio of correct answers was 66.67% for rose, 63.33% for mint, and 50% for chicory water.

## Discussion

The developed concept showed the potential of using DMF in OD. In future designs, the evaporator part should be integrated into the DMF module to decrease the response time. Also, the DMF driver board needs to be redesigned to have a better power supply for handling multiple odor droplets to have a shorter response time. Furthermore, a standard library of materials needs to be developed to have a strong smell to make it easier for humans to perceive and differentiate. This work can be a starting point for multidisciplinary collaborations across healthcare, psychology, microfabrication, and computer science.

## References

1. R. J. Stevenson, "Olfactory perception, cognition, and dysfunction in humans," WIRES Cognitive Science, vol. 4, no. 3, pp. 273–284, May 2013, doi: 10.1002/wcs.1224.
2. J. Tewell, "A Review of Olfactory Display Designs for Virtual Reality Environments," ACM vol. 56, no. 11, pp. 1–35, Nov. 2024, doi: 10.1145/3665243.

# OBJECTIVE RADIOTHERAPY TREATMENT PLAN EVALUATION TOOL TO SUPPORT PLANNING AUTOMATION

**Hiran CG Maladenige (1,2), Janne Heikkilä (2), Henri Korkalainen (1,2)**

*1. University of Eastern Finland, Department of Technical Physics, Finland; 2. Kuopio University Hospital, Cancer Centre, Finland*

## Introduction

Advancements in radiotherapy have increased treatment planning complexity, leading to variability and subjectivity in treatment plans. While deep learning is currently being explored to automate treatment planning [1], plan evaluation and comparison remain time-consuming and subjective due to the essential human involvement, hindering efficiency. To address this, we developed an objective tool for evaluating treatment plan quality using quantitative and qualitative features extracted from dose-volume histograms (DVHs), aligning with the consensus that DVHs are key indicators of plan performance [2].

## Methods

We developed a novel mathematical model, the advanced dose distribution index (ADDI), to evaluate plan quality. It utilises DVHs, organ-at-risk (OAR) dose constraints from literature, and Lyman's volume dependency of dose factor ($L_n$) [3] for each OAR. Then, it calculates the relevant target and OAR dose metrics including homogeneity, conformity, maximum dose ($D_{0.05cc}$), dose coverage ($D_{95\%}$) and comparative score of the real DVH with respect to OAR dose-volume limits. Finally, it expresses the plan quality as a polar vector, ADDI($r$, $\theta$), where $r$ reflects the overall quality while $\theta$ indicates the relative score of the target and OAR doses with ADDI(*1*, *45°*) representing the ideal case.

## Results

We applied the new ADDI and its proposed graphical representation to evaluate and compare tentative treatment plans. It captures the clinically relevant differences in the DVHs depending on the OAR and target dose constraints.

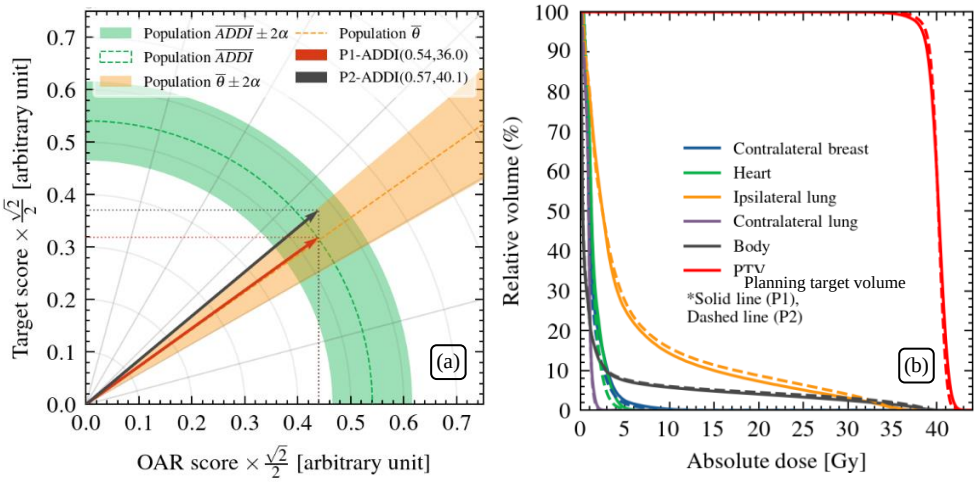


*Figure 1: (a) Example comparison of two tentative treatment plans (P1 & P2) for a left breast cancer patient using advanced dose distribution index (ADDI). The cartesian coordinates represent the normalised individual target and organ-at-risk scores. The coloured bands represent the mean ADDI(r,θ) for the approved plans for similar patients ± the standard deviation (σ). Dose-volume histograms of P1 & P2 are represented in (b).*

## Discussion

ADDI simplifies treatment plan evaluation and tentative plan comparison by concentrating clinically relevant aspects into a convenient polar vector. It provides added depth to DVH analysis and plan optimisation by allowing comparisons against a population. Its quantitative and graphical nature supports manual workflow and potentially assists automated workflows. ADDI should be tested and validated against a larger patient pool to understand its clinical applicability.

## References

1. A. Leino et al., Med Phys, 51,11:7986–7997, 2024.
2. L. J. C. Alfonso et al., Radiation Oncology, 10,1:1–9, 2015.
3. J. T. Lyman et al., Radiat Res Suppl, 8, 1985.

# DETECTION OF INFECTIOUS RESPIRATORY DISEASES USING WEARABLE DEVICES

**Inka Mustajoki, Katri Karhinoja (supervisor), Matti Kaisti (supervisor)**
*University of Turku*

## Introduction

Wearable devices are consumer worn devices that can be used to measure the body's physiological responses. Wearable devices are often non-invasive, for example worn on the wrist or finger, and can be used to measure heart rate, steps, respiratory rate, and several other parameters. Respiratory tract infections are common diseases, and their severity can vary from mild, like runny nose, to life-threatening pneumonia. In particular, the coronavirus that spread as a pandemic in 2020, caused plenty of deaths and lots of grief to society. During respiratory infections, the body undergoes physiological changes in response to activation of the immune system and those changes, for example raised resting heart rate (RHR), can be measured, for example via wearables. The purpose of this thesis was to find out, if the data from wearable devices can be used to detect a respiratory infection even before its symptom onset.

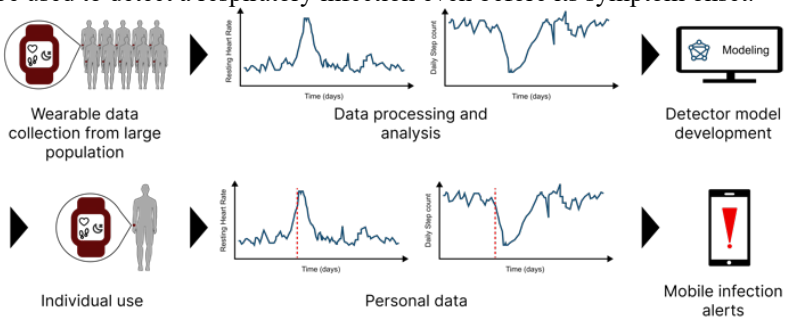


*Figure 1: Concept of detecting respiratory infections using wearable devices.*

## Methods

Three different earlier published anomaly detectors were applied to three open datasets also providing codes [1,2,3]. Resting heart rate, step count, heart rate variability and temperature were used as parameters. The datasets were open datasets published during COVID-19 pandemia, and the data were collected with commercial wearable devices. As for the detectors, Elliptic Envelope, Isolation Forest, and Finite State Machine based Night Signal from previous studies were used [1,2]. Different windows for diseased periods, i.e. true positive period, were tested.

## Results

Overall, the impact of infection on resting heart rate varied considerably between individuals. Sensitivities of all the detectors were low, around 20%. Different combinations of model parameters were tested to optimize the results, and sensitivity increased up to 50%, though with potential overfitting. Additionally, specificities and accuracies were relatively high regardless to the dataset or the detector, despite a notable number of false positives. Summary of detection results is shown in Table 1.

*Table 1: Performance summary of anomaly detectors for infection detection.*

| Detector | Sensitivity | Specificity | Accuracy |
|---|---|---|---|
| RHRAD | 19.2 % | 90.9% | 84.1% |
| Isolation Forest | 10.0% | 95.5% | 87.4% |
| Night Signal | 22.3% | 91.0% | 84.9% |

## Discussion

The possible explanation for the low sensitivity of the detectors is that physiological alterations caused by infections are similar with other physiological reactions, for example stress. With more complex models and using several measurable parameters at the same time, it might be possible to identify respiratory infections more reliably with wearable devices.

## References

1. Mishra, T, et al. "Pre-symptomatic detection of COVID-19 from smartwatch data." Nature biomedical engineering 4.12 (2020): 1208-1220.
2. Alavi, A, et al. "Real-time alerting system for COVID-19 and other stress events using wearable data." Nature medicine 28.1 (2022): 175-184.
3. Smarr, B. L., et al. "Feasibility of continuous fever monitoring using wearable devices." Scientific reports 10.1 (2020): 21640.

# COMPUTATIONAL MODELLING OF BRAIN ENERGY METABOLISM IN SCHIZOPHRENIA

**Ilona Mäkinen, Marja-Leena Linne, Tuomo Mäki-Marttunen**

*Tampere University, Finland*

## Introduction

Schizophrenia is a psychiatric disorder which affects 0.45 % of adults globally [1]. The cause of schizophrenia is not fully understood, but dysregulation of multiple neurotransmitters, environmental factors and genetics contribute to the disorder [2]. Schizophrenia has also been linked to abnormalities in brain energy metabolism which can cause dysregulation of synaptic activity [2]. That is why the aim of this thesis was to examine how the expression of cytosolic energy metabolism genes affects the concentrations of key energy metabolites in neurons and astrocytes in response to neuronal stimulus.

## Methods

Differential expression (DE) analysis was used to study the gene expression differences between schizophrenia patients (SCZ) and healthy controls (HC). The DE analysis used post-mortem bulk RNA sequencing data from the prefrontal cortex (PFC) and the anterior cingulate cortex (ACC) of the human brain [3]. Cell-type specific gene expressions were estimated by using CIBERSORTx tool. A computational model of brain energy metabolism [4] and Copasi simulator were used to simulate the gene expression changes and study their effect on central energy metabolite concentrations.

## Results

The DE analysis showed that there are 3 upregulated genes in the ACC and 7 in the PFC, and 6 downregulated genes in the ACC and 16 in the PFC in SCZ vs HC. The single-gene simulations showed that altered expression of most genes did not cause significant changes in any metabolite concentrations. However, decreased expression of neuronal genes PFKM in the PFC and LDHB in the ACC caused some significant alterations in the metabolite concentrations (Figure 1).

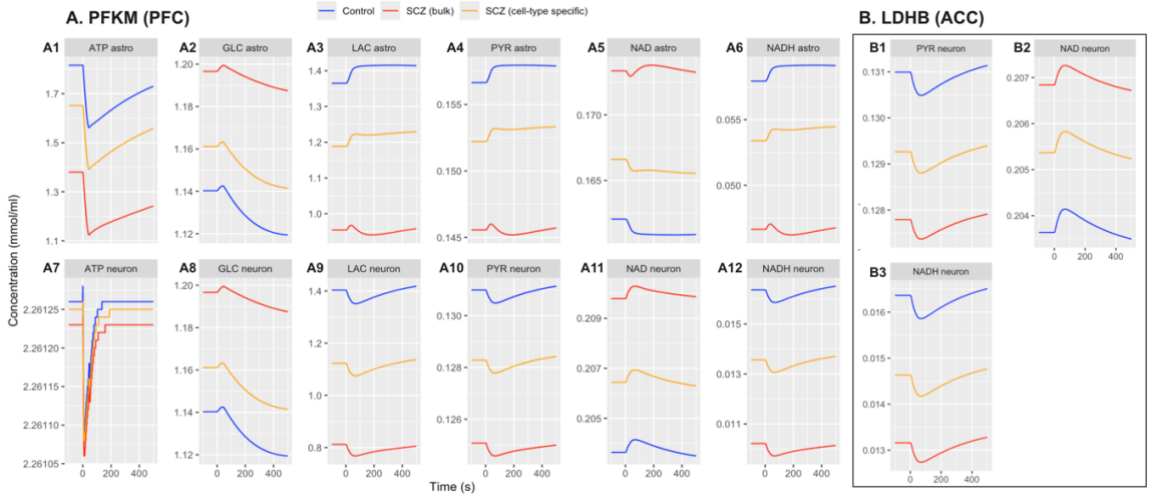


*Figure 1. Simulation results of genes with significant effect on the metabolite concentrations: PFKM (A1-A12) and LDHB (B1-B3). Neuronal stimulus occurs at t = 0 s. Glucose (GLC), lactate (LAC), pyruvate (PYR), astrocyte (astro).*

## Discussion

The DE analysis revealed region-specific bioenergetic dysregulation and supports the hypofrontality hypothesis of lower energy metabolism in frontal areas of the schizophrenic brain [5]. The simulation results showed that downregulation of two important glycolysis enzymes caused significant alterations in bioenergetics in SCZ. The use of these novel methods increases our knowledge of bioenergetics of schizophrenia and can provide new targets for personalized treatment.

## References

1. Institute of health Metrics and Evaluation (IHME). Global Health Data Exchange (GHDx). http://ghdx.healthdata.org/gbd-results-tool?params=gbd-api-2019-permalink/27a7644e8ad28e739382d31e77589dd7 (Accessed 3.2.2025).
2. C. R. Sullivan et al., Biol Psychiatry, 83:739-750, 2018.
3. G. E. Hoffman et al., Sci Data, 6:180, 2019.
4. F. Winter et al., J Cereb Blood Flow Metab, 8:304-316, 2018.
5. L. Townsend et al., Psychol Med, 53:4880-4897, 2023.

# THE EFFECT OF ALD COATING COMPOSITION ON COATING ADHESION AND IN VITRO DEGRADATION OF ORTHOPEDIC MAGNESIUM ALLOY IMPLANTS

**Lotta Mäkinen (1)**

*1. Tampere University, Finland*

## Introduction

Magnesium is a promising material for bioabsorbable orthopedic implants due to its mechanical properties close to those of bone, and biocompatibility [1], [2], [3]. However, the degradation of magnesium-based implants in physiological conditions is fast, difficult to predict, and causes hydrogen gas formation in the surrounding tissues [4], [5], [6]. To overcome these challenges, coatings for corrosion protection with good adhesion properties are developed. The aim of this work was to develop coating adhesion testing for atomic layer deposition (ALD) coated Mg-Ca-Zn alloy discs and orthopedic screws, and to compare the *in vitro* degradation rate and coating adhesion between three different coating compositions (A, B, and C, with similar thickness) on the magnesium alloy samples.

## Methods

**In vitro:** A 26-week *in vitro* degradation test for coated magnesium alloy discs was performed in modified Hank's buffer solution for all three coating compositions.
**Coating adhesion:** The coating adhesion testing of coated magnesium alloy discs was performed by a tape test modified from standard ASTM D3359-23 [7]. All coating compositions were included. Additionally, the coating adhesion on orthopedic magnesium alloy screws was tested. Coating compositions B and C were selected for the testing. The adhesion test included coated screw insertion into artificial bone to mimic the conditions of a surgical operation.

## Results

**In vitro:** At 2-week time point, the highest mass loss was observed with discs coated with coating C (comparable to the uncoated controls), whereas the discs coated with coatings A and B degraded slower. At 26-week time point, the results were the opposite.
**Coating adhesion:** *Discs:* No distinctive differences between the coating compositions were observed. Only <1 % of coating was detached during testing for all samples, indicating good coating adhesion. *Screws:* The testing revealed that the coating was most vulnerable for detachment in the screw threads that were in contact with artificial bone. In the screw shaft, most of the coating was retained during testing. There were no clear differences in the coating adhesion between the two studied coating compositions.

## Discussion

Based on the *in vitro* degradation and coating adhesion testing, the most promising coating for short-term corrosion protection was coating B, and for long-term protection, coating C. Short-term protection is more important in terms of orthopedic implant applications since after implantation, the mechanical properties of the implant need to be maintained long enough for the bone tissue to heal [8]. The testing provided important preliminary information of the ALD coating adhesion on magnesium alloy substrate. Based on this work, ALD coatings are a promising option for slowing down the degradation of magnesium based orthopedic implants.

## References

1. J. L. Wang, J. K. Xu, C. Hopkins, D. H. K. Chow, and L. Qin, "Biodegradable Magnesium-Based Implants in Orthopedics—A General Review and Perspectives," *Adv. Sci.*, vol. 7, no. 8, 2020, doi: 10.1002/advs.201902443.
2. A. Myrissa *et al.*, "In vitro and in vivo comparison of binary Mg alloys and pure Mg," *Mater. Sci. Eng. C*, vol. 61, pp. 865–874, 2016, doi: 10.1016/j.msec.2015.12.064.
3. R. B. Heimann, "Magnesium alloys for biomedical application: Advanced corrosion control through surface coating," *Surf. Coat. Technol.*, vol. 405, p. 126521, Jan. 2021, doi: 10.1016/j.surfcoat.2020.126521.
4. Y. Lu, S. Deshmukh, I. Jones, and Y.-L. Chiu, "Biodegradable magnesium alloys for orthopaedic applications," *Biomater. Transl.*, vol. 2, no. 3, pp. 214–235, 2021, doi: 10.12336/biomatertransl.2021.03.005.
5. G. Song, "Control of biodegradation of biocompatable magnesium alloys," *Corros. Sci.*, vol. 49, no. 4, pp. 1696–1701, 2007, doi: https://doi.org/10.1016/j.corsci.2007.01.001.
6. P. H. Quan *et al.*, "Fluoride Treatment and In Vitro Corrosion Behavior of Mg-Nd-Y-Zn-Zr Alloys Type," *Mater. Basel Switz.*, vol. 15, no. 2, p. 566, Jan. 2022, doi: 10.3390/ma15020566.
7. "ASTM D3359-23 Standard Test Methods for Rating Adhesion by Tape Test," ASTM International, Sep. 2023. doi: 10.1520/D3359-23.
8. B. Caldwell, "Everything You Need to Know About Fractures and Fracture Healing," Northern Arizona Orthopaedics. Accessed: Jun. 28, 2024. [Online]. Available: https://northazortho.com/ask-the-expert/everything-you-need-to-know-about-fractures-and-fracture-healing/

# DETERMINING THE CIRCULATORY RESPONSES RELATED TO RESPIRATORY EVENTS FROM THE PHOTOPLETHYSMOGRAM

**Jutta Nurminen (1,2), Salla Hietakoste (1,2), Samu Kainulainen (1,2)**

*1. Department of Technical Physics, University of Eastern Finland, Kuopio, Finland; 2. Diagnostic Imaging Center, Kuopio University Hospital, Kuopio, Finland*

## Introduction

Complete (apnea) and partial (hypopnea) breathing cessations in obstructive sleep apnea (OSA) cause various symptoms, including vasoconstriction, stiffening of blood vessels, and increased systemic vascular resistance[1]. Earlier studies have shown the relation between photoplethysmography (PPG) waveform and the condition of the circulatory system [2–4]. The amplitude difference between the systolic peak and dicrotic notch indicates vasomotor tone, with the movement of the dicrotic notch towards the systolic peak describing vasoconstriction [3]. Additionally, full width at half maximum (FWHM) of PPG waveform indicates systemic vascular resistance (SVR), where increased FWHM signifies increased SVR [2–4]. However, it is not known whether the severity of individual respiratory events has an acute modulatory effect on the photoplethysmogram (PPG) waveform. For these reasons, this Master's thesis aimed to investigate how the type and duration of respiratory events affect the PPG waveform.

## Methods

PPG waveform analysis was performed retrospectively for 520 OSA patients. Each respiration event was determined by using timestamps (starting point and duration), and the 10 s segment immediately before and after the respiratory event (pre- and post-segments) was determined based on these. From the PPG waveforms of the segments, the relative amplitude difference between the dicrotic notch and the systolic peak (ΔArel), and the FWHM of the whole pulse peak were determined. Respiratory events were separated into three groups depending on the duration of the event: 10 s–20 s, 20 s–30 s, and ≥ 30 s. These PPG waveform parameters were compared between 1) pre-, within-, and post-segments, 2) duration groups, and 3) types, so apneas and hypopneas.

## Results

In apneas and hypopneas, ΔArel and FWHM increased from the pre-respiratory event segment to the within-event segment ($p < 0.001$). In addition, in both event types, increasing respiratory event duration increased ΔArel and FWHM, in apneas from 0.560 to 0.585, from 429.7 ms to 437.5 ms, respectively ($p < 0.001$) and in hypopneas from 0.528 to 0.554, and from 402.3 ms to 429.7 ms, respectively ($p < 0.001$). These findings were more pronounced during apneas than hypopneas ($p < 0.001$). Generally, PPG waveform parameters returned to pre-segment levels after the events. In addition, the changes were greater during longer respiratory events and apneas.

## Discussion

The results of this Master's thesis show that respiratory events cause systematic changes to the PPG waveforms and are modulated by the type and duration of the event. These PPG waveform changes indicate vasoconstriction and systemic vascular resistance signifying an increased risk of cardiovascular diseases. Hence, PPG analysis could be utilized to evaluate the physiological stress of OSA.

## References

1 Dewan NA, Nieto FJ, Somers VK. Intermittent hypoxemia and OSA: implications for comorbidities. *Chest* American College of Chest Physicians; 2015; 147: 266–274.

2 Allen J. Photoplethysmography and its application in clinical physiological measurement. Physiol Meas Institute of Physics Publishing; 2007.

3 Murray WB, Anthony P. THE PERIPHERAL PULSE WAVE: INFORMATION OVERLOOKED. *Journal of clinical monitoring* 1996; 12: 365–377.

4 Awad AA, Haddadin AS, Tantawy H, *et al.* The relationship between the photoplethysmographic waveform and systemic vascular resistance. *J Clin Monit Comput* Springer; 2007; 21: 365–372.

## Acknowledgements

Financial support for the study was provided by Kuopio University Hospital and several Finnish private foundations. The authors thank Brett Duce (Princess Alexandra Hospital, Brisbane, Australia) for providing the PSG data for our analyses.

# SIGNAL-TO-EQUIVALENT THICKNESS CALIBRATION IMPROVES SOFT TISSUE CONTRAST WITH DIAGNOSTIC CBCT

**Samuel Onnela[1,2], Sampo Ylisiurua[1], Alexander Meaney[2]**

*1. University of Oulu; 2. University of Helsinki.*

## Introduction

Cone beam computed tomography (CBCT) X-ray imaging suffers from poor soft-tissue contrast, Hounsfield Unit (HU) instability and beam hardening -related artifacts [1]. The widely used flat-field correction (FFC) method for X-ray panel calibration is insufficient to correct these problems. This study aims to alleviate these issues using a signal-to-equivalent thickness calibration (STC) method [2,3].

## Methods

For STC calibration, acrylic of varying thicknesses was imaged to derive pixel-specific calibration curves for tube voltages of 80, 100, and 120 kV, utilizing a dental head-neck CBCT device. A spectral CT phantom with soft-tissue, calcification, and iodine targets was scanned under different parameters, and projection data corrected using FFC and STC before Feldkamp-Davis-Kress reconstruction. STC's impact on image quality was compared to FFC and the CBCT vendor's pipeline using contrast, HU values, and cupping artifact magnitude.

**Figures:**

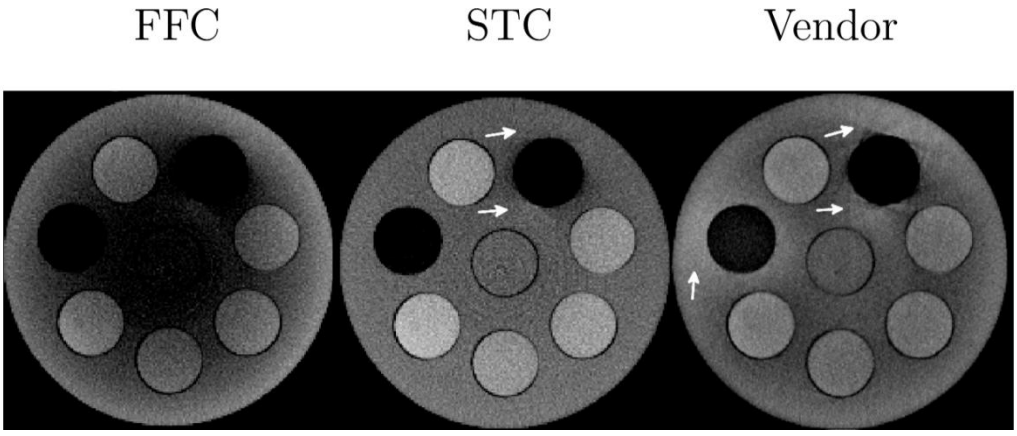


*Figure 1: QRM Spectral Phantom II with soft tissue inserts with narrow windowing FFC, STC, and Vendor images, from left to right, respectively. The narrow windowing setting: (center: 20 HU, width 200 HU). Arrows illustrate the halo and artefacts around lung (top-right) and adipose (middle-left) targets.*

## Results

STC enhanced soft tissue contrast by 33–77%, with the greatest improvement at 80 kV, except for adipose tissue. Contrast with STC also aligned more closely with the ground truth from the phantom vendor. For hard tissue and lung targets, STC showed slight improvement over FFC but no advantage over the vendor's reconstruction, which yielded the highest hard tissue contrast. STC reduced cupping artifacts compared to FFC but not the vendor's method.

## Discussion

The HU scaling was done using the measured phantom itself to scale the water HU levels closer to zero near the targets and thus highlight the effects of beam hardening in the material. Future work should hold the investigation of the impact of STC when scaling the reconstructions from separate measurements, in clinically relevant scenarios such as varying FOVs and larger and anthropomorphic phantoms, and other calibration materials such as aluminum.

## References

1. Loubele M, Maes F, Jacobs R, van Steenberghe D, White SC, Suetens P. Comparative study of image quality for MSCT and CBCT scanners for dentomaxillofacial radiology applications. Radiat Prot Dosimetry. 2008;
2. Vavrik, Daniel & Jakubek, Jan. (2009). Radiogram enhancement and linearization using the beam hardening correction method. NUCL INSTRUM METH PHYS RES A.
3. Gustschin, Nikolai & Gustschin, Alex & Epple, Michael & Allner, S. & Achterhold, Klaus & Herzen, Julia & Pfeiffer, Franz. (2019). Signal-to-thickness calibration and pixel-wise interpolation for beam-hardening artefact reduction in microCT. EPL

## Acknowledgements

The thesis was examined by Professor Sauli Savolainen and PhD Mikael Brix. The master's thesis work was extended into a manuscript yet to be published with co-authors of Sampo Ylisiurua, Alexander Meaney, Samuli Siltanen, Miika Nieminen and Mikael Brix.

# UTILISING FOURIER NEURAL OPERATORS FOR ULTRASOUND FIELD SIMULATIONS IN PHOTOACOUSTIC TOMOGRAPHY

**K. Puronhaara*[,1], T. Sahlström[1], A. Hauptmann[2] and T. Tarvainen[1]**
*[1]University of Eastern Finland, Kuopio, Finland; [2]University of Oulu, Oulu, Finland*
**karoliina.puronhaara@uef.fi*

## Introduction

Photoacoustic tomography (PAT) is an imaging modality that utilises photoacoustic effect [1]. In PAT, a short light pulse is used to illuminate the imaged target inducing a temperature increase due to absorption of light. The temperature increase is followed by localised pressure increase that relaxes as ultrasound waves. These waves propagate to the boundary of the target where they are measured using ultrasound sensors. A photoacoustic image is reconstructed from the measured ultrasound signals. Reconstructing PAT images can be time-consuming due to the need for simulating the propagation of ultrasound waves. The ultrasound waves are typically simulated using the finite difference, finite element, or pseudospectral *k*-space method, which can be computationally expensive, especially in three dimensions [2]. Deep learning-based methods offer a promising way to reduce the computational cost of ultrasound simulations, especially in iterative reconstruction methods where the simulations are performed repeatedly.

## Methods

In this work, simulation of ultrasound fields in PAT is studied using a deep learning-based Fourier neural operator (FNO) [3]. Ultrasound fields simulated with the FNO are compared to those obtained using the pseudospectral *k*-space method. The FNO is trained using ultrasound data simulated using blood vessel mimicking phantoms. In addition, its performance and ability to generalise is evaluated using two separate testing datasets.

## Results

An example of the results is shown in Figure 1. Ultrasound fields simulated with the FNO is compared to the pseudospectral *k*-space method using k-Wave toolbox [2].

## Discussion

The results indicates that the FNO can generate photoacoustic fields with a small error compared to the pseudospectral *k*-space method. In addition, the FNO is able to generalise well to data outside the training dataset.

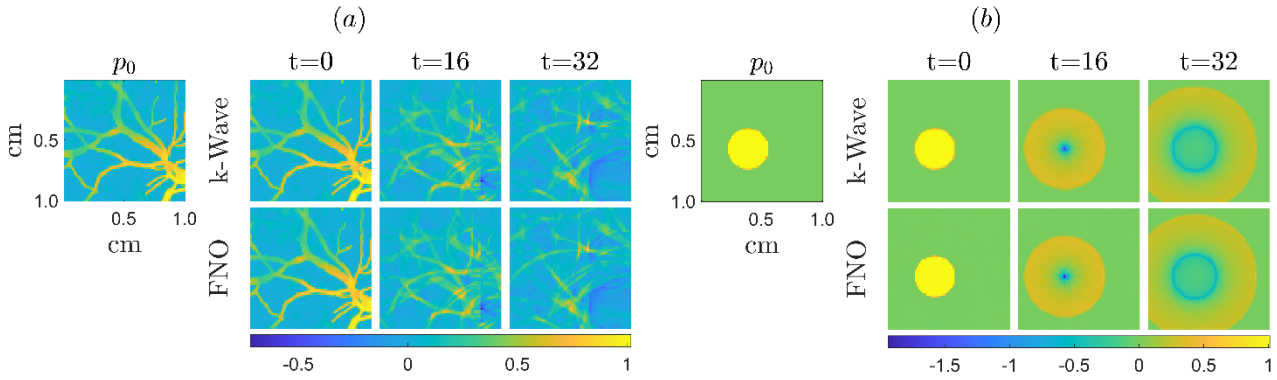


*Figure 1: Comparison of ultrasound waves from an initial pressure $p_0$ for three time points using the pseudospectral k-space method and the FNO for one sample from (a) the vessel and (b) the circle testing dataset.*

## References

1. P. Beard, Biomedical photoacoustic imaging, Interface Focus, 1:602–31, 2011.
2. B. Treeby and B.T. Cox. k-Wave: MATLAB toolbox for the simulation and reconstruction of photoacoustic wave fields, Journal of Biomedical Optics, 15(2):021314, 2010.
3. Z. Li, et al., Fourier neural operator for parametric partial differential equations, International Conference on Learning Representations (ICLR), 2021.

# MEDICAL DEVICE REGULATIONS: COMPARATIVE STUDY BETWEEN THE EU AND ASIA

**Niia Pöntinen**

*Tampere University, Finland*

## Introduction

The growing demand for medical devices in Asia, driven by aging populations and the rising prevalence of chronic diseases, presents significant opportunities for foreign manufacturers [1]. However, regulations governing the manufacturing, import, and sale of medical devices in the region are complex, and information related to the requirements is scattered and sometimes limited. For manufacturers in the European Union (EU), knowledge of the area is important in identifying market opportunities and planning a go-to-market strategy. This study reviewed the current state of medical device regulations in Asia and compared them with the Medical Device Regulation (MDR) of the EU. In order to do so, key regulatory elements namely definition of medical device, classification system, quality management system, pre-market approval procedures, and post-market controls were compared.

## Methods

The research was qualitative in nature and utilized a comparative study method. The study consisted of two phases. First, information on Asia as a whole was collected. This included the regulatory authorities, relevant regulations, and size of the medical device market in 48 countries. The collected data was further applied as the selection criteria for the countries included in the comparative analysis. As a result, the following countries were taken into closer examination: India, Pakistan, Japan, South Korea, Singapore, Malaysia, Thailand, and Saudi Arabia. For the second phase of the study, regulatory documents were collected from online sources, namely the official websites of the regulatory authorities of each country. The documents included laws, regulations, rules, notifications, and guidance documents. After extracting relevant information from the documents, a comparison between the countries and the EU was carried out.

## Results

Among the studied countries, variation was observed in the definitions of the term medical device. Although the definitions were generally similar to the EU one, differences were observed in the intended use and scope of the devices. While some countries had included veterinary products under the regulations, others lacked devices meant for support of conception or aid for disabilities. Consequently, not all products classified as medical devices in the EU constitute as such in the examined Asian countries. For classification systems, fewer differences were observed. All the countries had a four-tiered, risk-based system, like the EU. The most distinct differences were observed in the pre-market pathways which presented great variance among the countries. None of the countries had the same approach as the EU, although similarities were found, for instance from Malaysia. As for quality management, most countries recognize the ISO 13485 standard as a means of complying with requirements, although some exceptions exist. Of the post-market controls, adverse event reporting had a similar approach among the countries, but the identified post-market surveillance systems were estimated to be less extensive compared to the EU. Comparative findings indicate that while some countries such as Saudi Arabia and Malaysia shared similar traits with the EU, none of the countries had the same requirements to a larger extent.

## Discussion

During the study, it became evident that regulations in the EU and Asia differ in many respects, yet similarities also exist. The findings in this work essentially relate to the level of harmonization in Asia. A distinct difference between the implementation of pre-market and post-market elements among the countries was observed during the study, the latter being less frequently applied. In fact, Badnjević et al. [2] found that PMS activities worldwide tend to be less harmonized compared to pre-market controls. Although additional research is still needed to develop a full picture of the regulatory elements in these countries, this study adds to our understanding of the regulatory landscape in Asia and offers some insights into the varying practices and features found in the region.

## References

1. A. Kaushik et al., J. Young Pharm. 2:101-106, 2010.
2. A. Badnjević et al., Technol. Health Care, 30:1315-29, 2022.

## Acknowledgements

This work was supported by Horizon Europe “BIOMATDB”, Grant No. 101058779.

# HYDROGEL SCREENING FOR 3D VASCULAR MODEL ON MICROFLUIDIC CHIP

**Kati Rinnekari (1,2), Janne T. Koivisto (2), Hanna Vuorenpää (1), Susanna Miettinen (1), and Minna Kellomäki (2)**

*1.Adult Stem Cells group, Faculty of Medicine and Health Technology, Tampere University, Tampere, Finland; 2. Biomaterials and Tissue Engineering group, Faculty of Medicine and Health Technology, Tampere University, Tampere, Finland*

## Introduction

Hydrogels are biomaterials which consist of crosslinked polymer networks, and they have ability to absorb large amounts of water. In addition, hydrogels allow perfusion and give structural support to the cells. Hydrogels are crucial element for three-dimensional (3D) cell models since they mimic the cells' natural 3D environment, extracellular matrix (ECM). [1] In addition, 3D cell models mimic native tissues better than 2D models and thus are better models for studying human physiology. Vasculature is responsible for transport of oxygen, nutrients and metabolites and is therefore essential for all living tissues in human body [2]. Overall, both hydrogels and vasculature are essential when creating organotypic *in vitro* models such as Organ-on-Chip and even Body-on-Chip applications.

## Methods

This study focused on analyzing hydrogel size change, including degradation, and shrinking or swelling, by measuring the size of the samples *in vitro* during cultivation, testing protease inhibitors' effects on hydrogel's degradation or size change, and using these hydrogels (± inhibitors) to support 3D vascularization on microfluidic chip, that is Vascularization-on-a-Chip. The tested hydrogels included fibrin (human), collagen I (rat tail), VitroCol® (human collagen I), TeloCol® (bovine Telocollagen I), gelatin-gellan gum (porcine skin, bacterial) and VitroGel® (xeno-free). First, human lung fibroblasts (WI-38) were cultured embedded in hydrogels for 10 days. The size change of the hydrogels was measured every day during cultivation period. The area of the samples was measured with tile scan imaging, and the thickness was measured by imaging fluorescent beads embedded in the hydrogels, and volume was calculated based on these measured values. Cell viability and morphology were analyzed with Live/Dead and cytochemical staining. In microfluidic chips, human bone marrow stem/stromal cells (BMSCs), and green fluorescent protein (GFP) tagged human umbilical vein endothelial cells (GFP-HUVECs) were cultured inside a hydrogel for 10 days in dynamic conditions. The cellular reorganization, vascularization and cell morphology were analyzed by imaging signals of GFP and immunocytochemical staining.

## Results

Hydrogels in static conditions in a well plate showed varying characteristics in both sample size changes and cell morphology including elongation and spreading of the cells. Functional inhibitors preventing the decrease in size or degradation of the tested hydrogels were discovered during the study. In microfluidic chip experiments with dynamic culture conditions, the inhibitors supported 3D vascularization. Vascular network formed in fibrin hydrogel appeared to be more mature compared to vascular network formed in other hydrogels.

## Discussion

In conclusion, a method to analyze hydrogel size change by using fluorescent bead imaging was created, the hydrogel degradation was decreased with inhibitors and fibrin showed to be the most promising hydrogel to support 3D vasculature maintenance on-chip.

## References

1. Drury, J. L. *et al. Biomaterials* 24, 4337–4351 (2003)
2. Henderson, A. R. *et al. Micromachines (Basel)* 11, 147- (2020)

## Acknowledgements

This study was funded by the Research Council of Finland, Tays Research Services, Wellbeing Services County of Pirkanmaa, and Tampere University Hospital. We thank Tampere CellTech Laboratories and Tampere Imaging Facility for their services. We thank lab technicians Anna-Maija Honkala and Sari Kalliokoski for technical assistance.

# FABRICATION AND CHARACTERIZATION OF OPTICAL-RESOLUTION PHOTOACOUSTIC MICROSCOPE

**Markus Tolvanen**
*Department of Technical Physics, University of Eastern Finland*

## Introduction

Photoacoustic (PA) imaging is a hybrid imaging method with high contrast and spatial resolution, based on the PA effect, where absorbed light generates an ultrasound (US) signal [1]. A PA image is formed by illuminating the sample with pulsed light and measuring the generated US. Photoacoustic microscopy (PAM) is one of the PA imaging techniques [2]. The lateral resolution of the method ranges from micrometers to tens of micrometers. The intrinsic chromophores provide contrast in the image. The sample is typically probed with a focused ultrasonic transducer (UT) and a focused laser beam. Typically, near-infrared, visible or even ultraviolet light source with low energy is used to induce the PA effect [3]. A reconstruction algorithm is not required for image formation. PAM can be further divided into two different techniques: acoustic-resolution and optical-resolution photoacoustic microscopy.

## Methods

In this work, an optical-resolution photoacoustic microscope was constructed and characterized in transmission mode. In transmission mode, illumination of the sample and the measurement of ultrasonic signals are detected from opposite sides of the target. The device uses a focused infrared laser diode (LD) driven by a laser pulser generating nanosecond pulses. Ultrasound generated by a laser beam are measured by a focused UT with a center frequency of 25 MHz. The measured signals are digitized and stored with a software-controlled USB oscilloscope. The imaged sample is scanned systematically with the motorized linear stages. The hardware controlled by software is responsible for synchronized operation of its components. The performance and reliability of the hardware were verified through characterization measurements. Finally, the overall operation was tested using a thin black fiber was used as a target, and its thickness was 100 µm.

## Results

The device was able to measure samples with a lateral resolution of 45 µm x 73 µm, and the axial resolution of 83 µm. The measured central frequency was 23.44 MHz. The energy of the light pulse at the sample interface was 67 nJ, corresponding to a fluence of 2.0 mJ/cm$^2$. Energy measured directly from the LD was 1.488 µJ, with the maximum energy of 1.514 µJ and the minimum energy of 1.466 µJ. During one hour measurement the maximum variability was only 1.7 %. The laser pulse duration was 21 ns, with a rise time of 11 ns and a fall time of 7 ns. The laser pulse width was systematically 10 ns shorter than the duration of laser driver signal. Thin fiber target was raster scanned over region 810 µm x 800 µm. The scanning process required approximately 31 minutes, with a step size of 10 µm.

## Discussion

The performance and reliability of the mechanics, hardware, and software were verified through characterization measurements. Expected results for PA signal, LD energy, and overall operation. The lateral resolution was lower than expected. For future development, the LD with smaller emitter could be changed to enhance lateral resolution. With greater later resolution, the device is suitable for cell and tissue imaging. For faster acquisition, the laser beam could be steered with galvo mirrors. The light source could also be tuned so that the wavelength can be adjusted between the UV and VIS-NIR-spectrum.

## References

[1] L. Wang and J. Yao, “A practical guide to photoacoustic tomography in the life sciences,” *Nature Methods*, vol. 7, no. 5, pp. 627-638, 2016.

[2] P. Beard, “Biomedical photoacoustic imaging,” *Interface focus*, vol. 1, no. 4, pp. 602-631, 2011.

[3] X. Li, V. T. C. Tsang, L. Kang, Y. Zhang and T. T. W. Wong, “High-speed high-resolution laser diode-based photoacoustic microscopy for in vivo microvasculature imaging,” *Visual Computing for Industry, Biomedicine, and Art*, vol. 4, pp. 1-6, 2021.

## Acknowledgements

This work is supported by the Finnish Ministry of Education and Culture’s pilot for Doctoral Programmes (Pilot project Mathematics of Sensing, Imaging and Modelling).

# QUANTIFYING AND ANALYZING UNCERTAINTY IN AUTOMATIC SLEEP STAGING WITH NEURAL NETWORKS

**Miika Vainikka (1,2)**
**Matias Rusanen (1,2), Samu Kainulainen (1,2), Riku Huttunen (1,2)**

*1. Department of Technical Physics, University of Eastern Finland, Kuopio, Finland*
*2. Diagnostic Imaging Center, Kuopio University Hospital, Kuopio, Finland*

## Introduction

In sleep studies, sleep is classified into five stages (wake, N1, N2, N3, REM). Sleep staging is performed by trained professionals who visually analyze electroencephalography (EEG), electro-oculography (EOG), and electromyography (EMG) signals recorded throughout the night. [1] However, this manual process is labor-intensive and prone to errors [2].

Neural network-based automatic sleep staging offers comparable reliability and superior time efficiency to manual sleep staging [2-3], but clinical adoption requires assessing prediction uncertainty for transparency. This thesis aimed to validate and compare different methods for quantifying the uncertainty of a convolutional neural network-based sleep staging model [3].

## Methods

Two models trained on the STAGES dataset were analyzed: the MD (Max Dropout) model, which included 11 dropout layers, and the CD (Classifier Dropout) model, which contained one dropout layer. The Monte Carlo (MC) dropout method [4] was used to sample model outputs, or hypnodensities, representing the probabilities of different sleep stages. To assess prediction uncertainty, thresholds for the average hypnodensity and the standard deviation across 30 samples were established. Additionally, a hypnodensity interval (HI) method was developed that simultaneously utilized the sample mean and standard deviation of hypnodensities to evaluate uncertainty (Figure 1). The methods were compared by assessing performance improvement in the DOD dataset when uncertain epochs were removed.

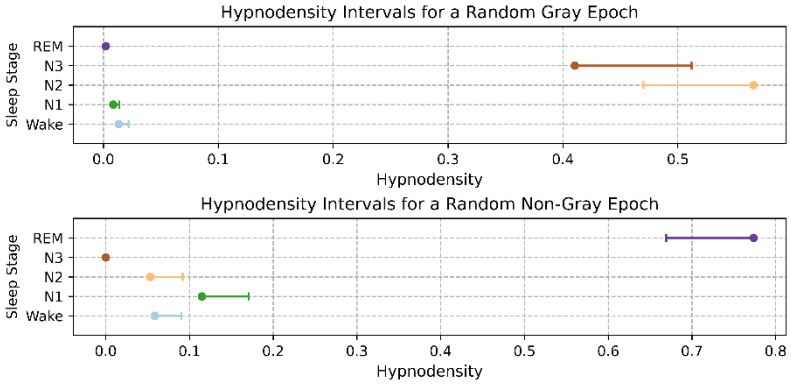


*Figure 1: Hypnodensity intervals predict the lower and upper bounds for the next MC dropout sample (e.g. 95% confidence). Overlapping intervals indicate uncertainty.*

## Results

Both models achieved an accuracy of at least 83 % in sleep staging. When excluding uncertain predictions, performance improved the most when using an average hypnodensity threshold, while improvement was least notable with a standard deviation threshold. The HI method performed similarly to the hypnodensity method, focusing more on the misclassifications between the N2 and N3 sleep stages. No significant difference in performance improvement was observed between the models.

## Discussion

We found that hypnodensities provide a reliable estimate of prediction uncertainty. The HI method, which does not rely on an arbitrary threshold, has also proven effective. These findings support the clinical adoption of automatic sleep staging by enhancing transparency and enabling manual review of uncertain sleep stages.

## References

1. Berry RB et al., AASM Scoring Manual Version 3.0, 2023
2. Phan H & Mikkelsen K, Physiol Meas. 43(4), 2022
3. Huttunen et al., IEEE Trans Biomed Eng. 70(5):1704-1714, 2023
4. Gal Y & Ghaharmani Z, PMLR 48:1050-1059, 2016

# NOT TOO HARMFUL, NOT TOO STILL BUT JUST RIGHT: CHARACTERISTICS OF AN ULTRASONIC TOOTHBRUSH [1]

**Sofia Annabella Voimanen (1)**

*1. Department of Biomedical Technology, Faculty of Medicine and Health Technology, Tampere University, Tampere, Finland*

## Introduction

Ultrasound safety is indicated by mechanical index and thermal increase of the tissues [2]. The mechanical index should not be over 0,7 so the ultrasound would be reasonably safe [2]. The ultrasound should not cause the temperature of tissue to rise more than 1,5 °C above the normal temperature [2, 3].

## Methods

The pressure signal of an ultrasonic toothbrush was measured with a hydrophone, which was under water and connected to an oscilloscope. The signal was measured from three different setups; the brush head under water, the handle under water and the brush head outside of the aquarium pressed against the aquarium glass (fig. 1). The temperature of the brush was measured nine times from the brush head and from the handle of the brush while the brush had been on.

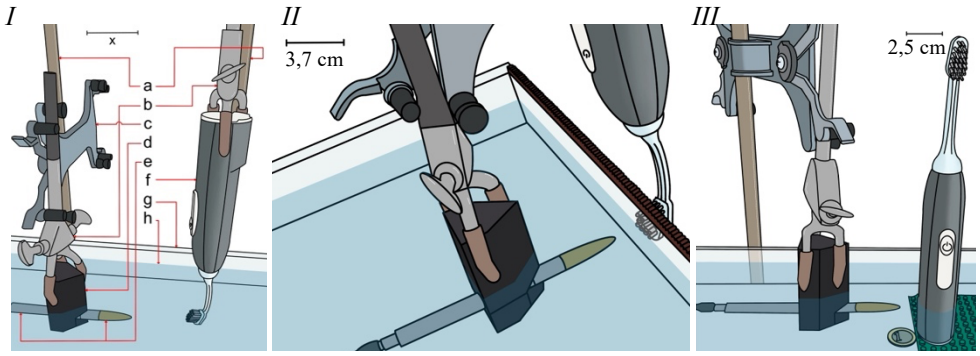


*Figure 1: (I) The setup, for measuring the signal, consisted of clamp stands, clamps and a clamp for hydrophone (a-d), a hydrophone (e), a toothbrush (f) and an aquarium (g) filled with water (h). The scale (x) is 4,1 cm. (II) The brush was also held outside of the aquarium. (III) On the third setup the toothbrush was standing on the bottom of the aquarium on a toy block platform next to a 1€ coin.*

## Results

The minimum pressure was -32,8 kPa for the brush head and -35,4 kPa for the handle. The measured frequencies were 420 kHz and 840 kHz. The mechanical index was 0,06 for the handle and for the brush head. The starting temperature of the brush head was 18,2 °C and starting temperature of the handle was 17,8 °C. The maximum temperature was 19,1 °C for the handle and for the brush head. The maximum temperature was achieved after 60 minutes.

## Discussion

The mechanical index was under the safety limit of 0,7 and the thermal increase of the brush was not too high. Based on the results of the experiments, the toothbrush does not produce ultrasound that causes damages.

## References

1. S. A. Voimanen, “Not too harmful, not too still but just right: characteristics of an ultrasonic toothbrush”, MSc thesis, Tampere University, 2024. Available: https://urn.fi/URN:NBN:fi:tuni-2024121211045.
2. F. A. Duck, “Medical and non-medical protection standards for ultrasound and infrasound”, Progress in Biophysics and Molecular Biology, 93.1–3:176–191, 2007, DOI: 10.1016/j.pbiomolbio.2006.07.008.
3. T. Nishikawa et al, “A study of the efficacy of ultrasonic waves in removing biofilms”, Gerodontology, 27:199–206, 2010, DOI: 10.1111/j.1741-2358.2009.00325.x.

## Acknowledgements

This work has been supported by the Deutsche Forschungsgemeinschaft (DFG) Emmy- Noether Programme, Grant Number 38355133, by the Academy of Finland, Grant Number 340026, and by the National Research Foundation of South Africa, Grant Number 127102. The author states no conflict of interest. The author states that informed consent is not applicable.

# CHANGES IN JOINT SPACE WIDTH AFTER DRASTIC WEIGHT LOSS

**Lassi Vuononvirta[1], Tom Turmezei[2,3], Tuomas Frondelius[1], Mika Nevalainen[1,4], Santeri Rytky[1,4], Juhani Määttä[1], Sanna Meriläinen[5,6], Petri Lehenkari[6,7], Mikko Finnilä[1,8]**

*1. Research Unit of Health Sciences and Technology, University of Oulu, Oulu, Finland. 2. Department of Radiology, Norfolk and Norwich University Hospitals NHS Foundation Trust, Norwich, United Kingdom. 3. Norwich Medical School, University of East Anglia, Norwich, United Kingdom. 4. Department of Diagnostic Radiology, Oulu University Hospital, Oulu, Finland. 5. Department of Anesthesiology, Surgery, and Intensive Care, Oulu University Hospital, Oulu, Finland. 6. Research Unit of Translational Medicine, University of Oulu, Oulu, Finland. 7. Medical Research Center Oulu, University of Oulu, Oulu, Finland. 8. Biocenter Oulu, University of Oulu, Oulu, Finland.*

## Introduction

Osteoarthritis (OA) is a leading joint disease, with obesity as a major risk factor[1]. Even a 5 kg weight loss can reduce knee OA risk by over 50%[2]. Joint space width (JSW) is a key OA indicator, but traditional radiography lacks sensitivity[3]. Advanced cone-beam-CT (CBCT) imaging, with joint space mapping, offers improved detection[4]. This study examines the impact of Roux-en-Y gastric bypass (RYGB) on JSW in OA patients, using advanced imaging to assess structural changes.

## Methods

Eighty-six individuals with obesity participated: 45 underwent Roux-en-Y gastric bypass (RYGB) surgery (BMI 42.5 ± 6.3 kg/m²), while 41 served as controls (BMI 39.4 ± 4.2 kg/m²). Weight-bearing CBCT scans (Planmed Verity, 0.2 mm voxel size) were acquired with patients standing under unilateral loading. Joint space width (JSW) mapping was performed by segmenting the femur and tibia (Stradview v7.21) and generating 3D JSW maps. Subregions were analyzed, and t-tests compared within-group changes over time and between-group differences at follow-up. Analyses considered weight loss success and Kellgren-Lawrence grading (KLG).

## Results

The conservative weight loss group showed no change in BMI. The RYGB group was divided into subgroups based on weight loss success: unsuccessful (BMI reduction <20%) and successful (BMI reduction >20%). In the subgroup with successful weight loss, a significant widening was observed in the central region and medial quarter of the medial condyle with a mean difference +0.13 ± 0.05 mm and +0.22 ± 0.23 mm, respectively (Fig 1). Those in RYGB group with KLG < 2 (n = 23) had significant wider joint space in the inner medial subregion by a mean of +0.13 ± 0.11 mm compared to control group. Patients with the KLG > 2 (n = 8) had significantly wider joint space in the posterior subregion of lateral compartment by a mean of +0.44 ± 0.23 mm compared to control group.

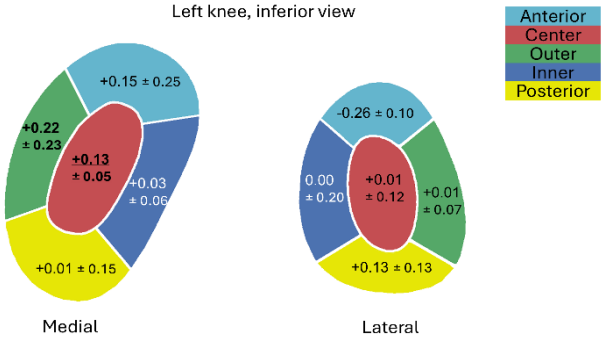


*Figure 1. Joint space width (JSW) mean and standard deviation change after 1 year (mm) for the successful weight loss mapped on the canonical joint surface and divided into subregions.*

## Discussion

Successful weight loss after RYGB is associated with a wider joint space in the central and inner regions of the medial tibiofemoral compartment at 1 year. The most likely reason for this finding is the relief of forces through the joint from weight loss that may result in less cartilage compression, meniscal extrusion, and deviation in knee alignment. The pattern of joint space change in the whole RYBG group after 1 year suggests a more complex relationship between bariatric surgery, joint space dynamics, and the development of osteoarthritis in the context of obesity.

## References

1. Long, H., Liu, Q., Yin, H., Wang, K., Diao, N., Zhang, Y., Lin, J., & Guo, A. (2022). Prevalence Trends of Site-Specific Osteoarthritis From 1990 to 2019: Findings From the Global Burden of Disease Study 2019. Arthritis and Rheumatology, 74(7).
2. Zheng, H., & Chen, C. (2015). Body mass index and risk of knee osteoarthritis: systematic review and meta-analysis of prospective studies. BMJ Open, 5(12), e007568.
3. Kellgren, J. H., & Lawrence, J. S. (1957). Radiological Assessment of Osteo-Arthrosis. Annals of the Rheumatic Diseases, 16(4), 494–502.
4. Turmezei, T. D., Low, S. B., Rupret, S., Treece, G. M., Gee, A. H., MacKay, J. W., Lynch, J. A., Poole, K. E. S., & Segal, N. A. (2021). Quantitative three-dimensional assessment of knee joint space width from weight-bearing CT. Radiology, 299(3), 649–659.

# STUDYING NOVEL PROPERTIES OF LEVOSIMENDAN METABOLITE OR-1896 ON ISCHEMIC HIPSC-DERIVED CARDIOMYOCYTES

**Kaisla Walls (1), Mari Pekkanen-Mattila (2), Katriina Aalto-Setälä (2,3)**

*1. Computational Biophysics and Imaging Group, Tampere University, Finland; 2. Heart Group, Tampere University, Finland; 3. Heart Hospital, Tampere University Hospital, Finland*

## Introduction

Acute myocardial infarction (AMI) is the leading cause mortality worldwide. The narrowing of coronary arteries and subsequential cessation of blood flow cause acute hypoxia to the myocardium, leading to changes in cell behavior, genesis of arrhythmias, and loss of function in the heart. Current pharmacological agents for treatment of arrhythmias during AMI are not recommended to be given prophylactically and have not been shown to exhibit clear efficacy in patients. Levosimendan, a positively inotropic $Ca^{2+}$ sensitizer currently used for acute decompensated heart failure, has been previously shown to have antiarrhythmic properties during hypoxia experiments. However, the active metabolite of levosimendan, OR-1896, has not been studied previously.

Traditionally, animal models have been used to study cardiac phenotypes in health and disease, but the differences in physiology and electrochemical properties cause limitations in their usability. Human-induced pluripotent stem cell-derived cardiomyocytes (hiPSC-CMs) provide a continuous source of human-derived cardiomyocytes for modelling cardiac diseases, and despite their limitations in maturity, hiPSC-CMs have previously been successfully used in multiple setups for modelling myocardial ischemia. In this thesis work, hiPSC-CMs are used in AMI model based on the setup presented by (Gaballah et al., 2022), and the effects of the active metabolite of levosimendan, OR-1896, are studied under acute hypoxia.

## Methods

Healthy hiPSC-derived cell line was used for cardiomyocyte differentiation. Differentiated and sorted hiPSC-CMs were cultured for 7 days prior to initiating hypoxia experiments in OxyGenie 1-well culture chambers (The Baker Company, USA). The addition of levosimendan (20 µM, Sigma-Aldrich, USA) and its metabolite OR-1896 (1-2 µM Orion, Finland) were studied against hypoxic control without treatment and normoxic control (21% $O_2$, 5% $CO_2$). Baseline measurements for calcium imaging were recorded, and the OxyGeniem mini-incubator (The Baker Company, USA) was used to inflict hypoxia (0% $O_2$, 5% $CO_2$, and 95% $N_2$). Calcium transients from each group i) normoxic control, ii) hypoxic control, iii) hypoxia with levosimendan, and iv) hypoxia with metabolite OR-1896 were recorded at 4 and 7 hours, and post-hypoxia media was collected for enzyme-linked immunosorbent assay (ELISA) for released cardiac protein cardiac troponin T (cTnT), indicating cardiac damage. Separate samples were prepared for immunostainings to visualize the effect of hypoxia to the morphology of cardiomyocytes, staining for cTnT, connexin-43, and α-actinin.

## Results

The results show that OR-1896 has significant antiarrhythmic effect in reducing the cases of arrhythmias seen in hypoxia without any treatment ($p<0.01$) and countering the effects in $Ca^{2+}$ kinetics in rise and decay time seen in hypoxia without treatment ($p<0.05$ and $p<0.001$, respectively). Additionally, OR-1896 showed a decrease in the amount of released cardiac troponin T (cTnT) and sustained cellular structures in immunostained samples, implicating known cardioprotective properties in this hiPSC-CM-derived platform for modelling AMI.

## Discussion

This thesis work shows novel antiarrhythmic properties of the active metabolite of levosimendan which suggest a new clinical use for the drug in the setting of AMI. Additionally, it provides evidence on the usability of hiPSC-CMs as a disease modelling tool, showing known cardioprotective effects of OR-1896 in cell culture. Future work still needs to be conducted on enhancing the level of maturation in hiPSC-CMs to better the model, and further studies are needed for determining the specific antiarrhythmic effect of OR-1896.

## References

Gaballah, M., Penttinen, K., Kreutzer, J., Mäki, A. J., Kallio, P., & Aalto-Setälä, K. (2022). Cardiac Ischemia On-a-Chip: Antiarrhythmic Effect of Levosimendan on Ischemic Human-Induced Pluripotent Stem Cell-Derived Cardiomyocytes. Cells, 11(6), 1045. https://doi.org/10.3390/cells11061045

# PhD Project Presentations

1. **UZMAN ALI ET AL.**, IMPLANT-TO-IMPLANT COMMUNICATIONS USING QUAD-BAND PIFAS FOR INTRACRANIAL APPLICATIONS

2. **ELOIS CANALS ET AL.**, PREDICTING CARTILAGE THICKNESS MAPS FROM MULTISPECTRAL IMAGING USING DEEP LEARNING

3. **AKUROMA GEORGE ET AL.**, DIFFUSE REFLECTANCE SPECTROSCOPY FOR CHARACTERIZATION OF TISSUE OPTICAL PROPERTIES

4. **SONYA GHANAVATI ET AL.**, BIOPHOTONIC COMPOSITE SCAFFOLDS FOR CONTROLLED NITRIC OXIDE RELEASE UPON NIR EXCITATION

5. **VIRGINIA ALESSANDRA GOBBO ET AL.**, IMPACT OF PROTEIN ADSORPTION ON BIOACTIVE GLASSES AND BIOLOGICAL RESPONSE: A STEP FORWARD TOWARDS A PREDICTABLE CELL FATE

6. **ATTE JOUTSEN**, DRY ELECTRODE SOLUTIONS FOR MEASURING CARDIAC ACTIVITY IN WEARABLE TECHNOLOGY

7. **HARINA KARUNARATHNA ET AL.**, ADAPTATION OF NEAR INFRARED SPECTROSCOPY FOR IN SITU MONITORING OF TISSUE ENGINEERED CARTILAGE GROWTH

8. **LAURA KETO ET AL.**, DECIPHERING CEREBELLAR ASTROGLIAL CALCIUM DYNAMICS WITH DETAILED WHOLE-CELL MODELING

9. **NITHIN SADEESH ET AL.**, INVESTIGATING THE EFFECTS OF INFLAMMATORY FACTORS ON JOINT TISSUES USING NEAR-INFRARED (NIR) SPECTROSCOPY ON EXPLANT CULTURE MEDIUM

10. **SEYED MAHAN NEMATOLLAHI SANIJ ET AL**., ESTIMATING KNEE JOINT CARTILAGE MECHANICS USING FINITE ELEMENT BY NEURAL NETWORK BASED KINETIC DATA

11. **SAANA SEPPÄLÄ ET AL**., IMPAIRED MEMORY STORAGE AND RECALL OF HIPPOCAMPAL CA1-CA3 NETWORK IN EARLY ALZHEIMER'S DISEASE

12. **KAISA TORNBERG ET AL**., COMBINING MICROFLUIDIC TECHNOLOGY WITH HUMAN BASED CELL MODELS TO BUILD BODY-ON-CHIP FOR STROKE-HEART SYNDROME

13. **KATJA TÖRMÄ ET AL**., MULTIVARIATE DIRECTED FUNCTIONAL CONNECTIVITY METHODS FOR ESTIMATION OF WHOLE-BRAIN CONNECTIVITY

# IMPLANT-TO-IMPLANT COMMUNICATIONS USING QUAD-BAND PIFAS FOR INTRACRANIAL APPLICATIONS

**Uzman Ali (1), Abdul Basir (1), Nasir Ullah Khan (1), Toni Björninen (1)**

1. *Tampere Electronics Research Centre, Tampere University, Tampere, Finland*

## Introduction

Wireless implantable medical devices enable real-time health monitoring and diagnostics. Implant-to-implant (I2I) communication further enhances their functionality by allowing direct data exchange between multiple implants. However, designing multiband efficient implantable antennas for I2I communication is challenging due to the lossy biological tissue environment and frequency detuning [1]. This study explores I2I communication using PIFAs designed for intracranial applications. The antenna operates in MedRadio (402 MHz), WMTS (1430 MHz), and ISM (915 and 2450 MHz) bands. Numerical simulations analyze reflection coefficient, mutual coupling, and gain performance at different implant depths in a seven-layer human head model. Results suggest that the 915 MHz band provides the best performance, making it the most suitable frequency for reliable I2I communication in brain-implanted systems.

## Methods

Numerical simulations were conducted using ANSYS HFSS to evaluate I2I communication between two quad-band PIFAs in a seven-layer human head model. One antenna was implanted 14.8 mm deep in the cerebrospinal fluid (CSF) layer, while the other was positioned 75 mm deep in the brain. A thin silicone coating is deployed on antenna for biocompatibility. The study analyzed the reflection coefficient (|S11|), mutual coupling (|S21|), and gain performance at four frequency bands. The impact of antenna rotation on electromagnetic coupling was also examined to determine the most suitable frequency for reliable I2I communication.

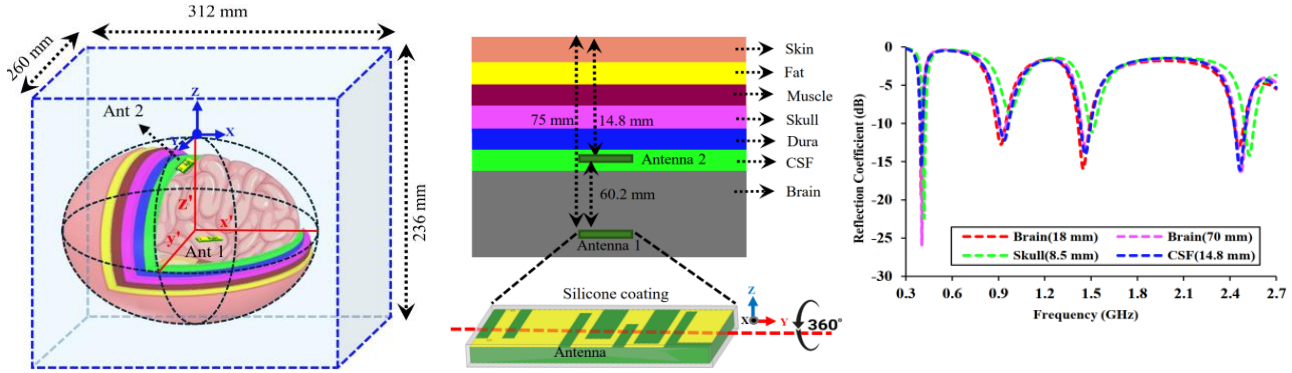


*Figure 1. (a) Simulation environment of I2I communication (b) cross-sectional view of 7-layer human head model (c) reflection coefficient of PIFA at different implant depths.*

## Results

The quad-band PIFA exhibited |S11| values below -10 dB across all bands, ensuring effective impedance matching. Mutual coupling (|S21|) and combined gain (G1*G2) showed a similar trend with rotation, with maximum values at 180°. Among the tested frequencies, the 915 MHz band demonstrated the highest coupling and gain, making it optimal for I2I communication. The 402 MHz band exhibited discrepancies in coupling prediction versus gain, requiring further investigation. The calculated wave impedance (|η|) aligned with expected values, validating the simulation model for reliable intracranial I2I communication analysis.

## Discussion

The study confirms that quad-band PIFA antennas can facilitate I2I communication in intracranial applications. The 915 MHz band exhibited optimal coupling and gain, making it the most suitable for reliable communication. However, deviations at 402 MHz indicate frequency-dependent challenges, necessitating further investigation through experimental validation and analytical modelling for enhanced performance.

## References

1. S. Gabriel, R. W. Lau, C. Gabriel, “The dielectric properties of biological tissues: III. Parametric models for the dielectric spectrum of tissues,” Phys. Med. Biol., vol. 41, no. 11, Nov. 1996.

# PREDICTING CARTILAGE THICKNESS MAPS FROM MULTISPECTRAL IMAGING USING DEEP LEARNING

**Eloi Canals Pascual[1,2], Hamidreza Masjedi[1,2], Akuroma George[1], Petri Paakkari[1,3], Arash Mirhashemi[1], Ervin Nippolainen[1], Juha Töyräs[1,2,4] , Isaac Afara[1,4]**

*1. Department of Technical Physics, University of Eastern Finland, Kuopio, Finland; 2. Kuopio University Hospital, Science Service Center, Kuopio, Finland; 3. Kuopio University Hospital, Diagnostic Imaging Center, Kuopio, Finland; 4. The University of Queensland, School of Electrical Engineering and Computer Science, Brisbane, Australia*

## Introduction

Articular cartilage (AC) is a smooth connective tissue covering articulating joint surfaces [1]. A complex disease of AC, known as osteoarthritis (OA), is characterized by pain, limited mobility, and cartilage degeneration [2]. OA can cause cartilage thickening especially in early stages, while in later stages, it often leads to cartilage thinning [3]. Predicting cartilage thickness has been proven to be feasible from its optical properties by reflectance spectroscopy [4], [5]. However, these studies were restricted to point measurements. To characterize AC properties, reflectance Multispectral Imaging (MSI) is shown to be a promising technique that captures both spatial and spectral information [6] . Yet, to our knowledge, the potential of MSI to estimate AC thickness distribution is unexplored. In this study, we aim to map bovine AC thickness using a custom-made MSI system.

## Methods

In the study, patellar samples of bovine knee joints ($n$ = 8) were harvested, stored frozen (–20ºC) in phosphate-buffered saline. Subsequently, specimens (1 cm x 2 cm) were extracted from the medial and lateral parts of each sample. The specimens were then imaged using a custom-made MSI device, equipped with six narrow-band LEDs (550–970 nm) and a CMOS camera sensor (1.31 megapixels, 5.20 µm pixel size). We captured spectral images of the specimens, collecting their reflectance spectra across the specified wavelength range. We derived cartilage thickness maps from micro-computed tomography images (Nikon Metrology, XT H 225, 50 $\mu m^3$ voxel size) using MATLAB. To predict the thickness, we implemented a supervised convolutional neural network (CNN) model based on the VGG architecture [7], which takes the MSI data cube as input and outputs thickness maps. The CNN was trained on a subset of the data, leaving one knee out for testing and using the remaining with 80–20% training–validation split. The code was run on the Puhti supercomputer using Python and TensorFlow. The performance of the model was assessed via the mean absolute error (MAE) metric.

## Results

The model predicted cartilage thickness maps from MSI images with a MAE of 0.08 mm for the train set and a MAE of 0.19 mm for the test set. Pearson's Correlation Coefficient (PCC) [8] between the predicted and ground truth maps was 0.85. The $R^2$ value was 0.52 and the Structural Similarity Index Metric (SSIM) [9] between the two maps was 0.23. Figure 1 presents initial predictions of thickness maps derived from the six-channel multispectral images.

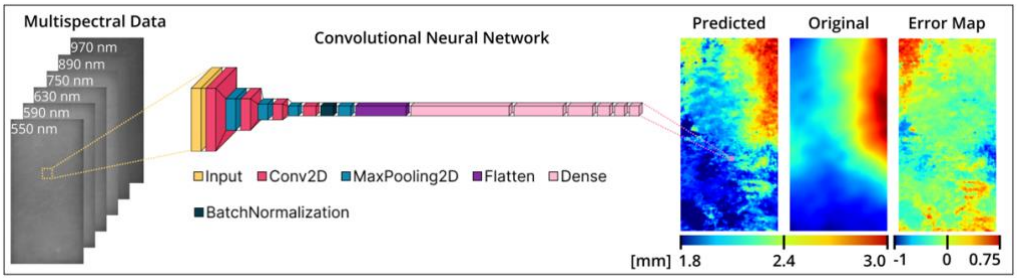


*Figure 1: Preliminary results of predicting the thickness map from multispectral images of the samples.*

## Discussion

The study demonstrates MSI's potential for predicting cartilage thickness maps, with a low MAE (0.19 mm) and strong PCC (0.85) indicating high linear agreement. However, the $R^2$ (0.52) and SSIM (0.23) suggest room for improvement in explaining variance and capturing fine details. While the model shows promise, further refinement and validation on larger datasets are needed to enhance accuracy and clinical applicability.

## References


1. A. J. Sophia Fox, A. Bedi, and S. A. Rodeo, “The basic science of articular cartilage: structure, composition, and function,” Sports Health, vol. 1, no. 6, pp. 461–468, 2009.
2. M. B. Goldring and S. R. Goldring, “Osteoarthritis,” Dec. 2007. doi: 10.1002/jcp.21258.
3. R. J. Buck, W. Wirth, D. Dreher, M. Nevitt, and F. Eckstein, “Frequency and spatial distribution of cartilage thickness change in knee osteoarthritis and its relation to clinical and radiographic covariates–data from the osteoarthritis initiative,” Osteoarthritis Cartilage, vol. 21, no. 1, pp. 102–109, 2013.
4. I. Afara, S. Singh, and A. Oloyede, “Application of near infrared (NIR) spectroscopy for determining the thickness of articular cartilage,” Med Eng Phys, vol. 35, no. 1, pp. 88–95, 2013.
5. A. Johansson, Å. Öberg, T. Sundqvist, and M. Sundberg, “Assessment of cartilage thickness utilising reflectance spectroscopy,” 2002.
6. J. Kinnunen, S. Saarakkala, M. Hauta-Kasari, P. Vahimaa, and J. S. Jurvelin, “Optical spectral reflectance of human articular cartilage–relationships with tissue structure, composition and mechanical properties,” Biomed Opt Express, vol. 2, no. 5, pp. 1394–1402, 2011.
7. Simonyan, Karen & Zisserman, Andrew. (2014). Very Deep Convolutional Networks for Large-Scale Image Recognition. arXiv 1409.1556.
8. Pearson, K. (1895). “Note on Regression and Inheritance in the Case of Two Parents.” *Proceedings of the Royal Society of London*, 58(347-352), 240–242.
9. Wang, Z., Bovik, A. C., Sheikh, H. R., & Simoncelli, E. P. (2004). “Image Quality Assessment: From Error Visibility to Structural Similarity.” *IEEE Transactions on Image Processing*, 13(4), 600–612.

# DIFFUSE REFLECTANCE SPECTROSCOPY FOR CHARACTERIZATION OF TISSUE OPTICAL PROPERTIES

Akuroma George[1], Iman Kafian-Attari[1], Ervin Nippolainen[1], Arash Mirhashemi[1], Isaac O. Afara[1,2]

*[1]Department of Technical Physics, University of Eastern Finland, Kuopio, Finland, [2] The University of Queensland, School of Electrical Engineering and Computer Science, Brisbane, Australia*

## Introduction

Osteoarthritis (OA) is a debilitating joint disease associated with severe pain, reduced mobility, and significant socio-economic impact. Affecting 28% of adults over 60 globally. In Finland, approximately 5-6% of the population is clinically diagnosed with hip OA[1], which contributes to some of Europe's highest rates of joint replacement surgeries. Despite the availability of joint repair techniques, their success relies heavily on accurately diagnosing the severity and extent of joint injuries. Current diagnostic methods for cartilage defects, such as arthroscopy, are widely used in knee and other joints but are highly subjective and poorly reproducible. However, arthroscopy is not commonly performed for hip osteoarthritis, necessitating the development of sensitive and quantitative tools for assessing cartilage integrity across different joint conditions. Recent advances in optical methods, such as near-infrared (NIR) spectroscopy, have shown promise for evaluating cartilage's physical, biomechanical, and biochemical properties[2]. However, there is insufficient knowledge of the interaction of light with articular cartilage and how its degeneration impacts optical properties. Understanding key optical properties, including absorption ($\mu_a$) and reduced scattering ($\mu_s'$) coefficients, are critical as these are intrinsically related to cartilage composition and structure. Given the depth-dependent complexity of cartilage, a comprehensive understanding of its optical properties is essential for interpreting and clinically translating optical spectroscopy for OA diagnosis. This study aims to develop and validate a non-destructive diffuse reflectance spectroscopy (DRS) approach for estimation of cartilage optical properties. The objective of this initial preliminary study was to assess the sensitivity of DRS to cartilage from different anatomical locations.

## Methods

Reflectance measurements were acquired using diffuse reflectance spectroscopy (DRS) from four rectangular bovine cartilage plugs, extracted from the patellae of four different knees (two right and two left). Each plug contained two anatomical regions: medial and lateral, with six measurement points per region, resulting in 12 measurements per plug. This yielded a total of 24 measurement points across all plugs for each anatomical region (medial: 12, lateral: 12). Spectral analysis was performed to examine regional differences in cartilage reflectance. Mean reflectance spectra were computed separately for medial and lateral regions, with the standard error of the mean (SEM) displayed as shaded regions in the spectral plots. The data were processed and visualised over a 450–750 nm wavelength range, comparing spectral trends between medial and lateral regions.

## Results

Samples from the lateral compartment showed an overall increase in reflectance compared to the medial compartment. This is likely due to differences in tissue composition and structure between these locations.

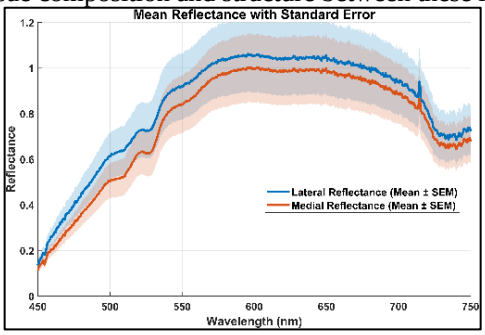


*Figure 1: Mean reflectance spectra (± standard error) for medial and lateral cartilage regions measured using diffuse reflectance spectroscopy.*

## Discussion

The observed increase in reflectance in the lateral compartment compared to the medial is likely due to differences in tissue composition and structure. Since the samples appeared visually intact, this trend is unlikely to be related to cartilage integrity, suggesting that intrinsic variations in composition or organization influence the optical response. These reflectance spectra provide valuable insights into regional optical differences in cartilage and serve as a foundation for estimating absorption and scattering properties using diffusion approximation theory.

## References


1. Development, O. for E. C. and. Health at a Glance: Europe 2022—Rates of Hip and Knee Replacements by Country. Preprint at https://www.oecd.org (2022).
2. Afara, I. O. *et al.* Characterization of connective tissues using near-infrared spectroscopy and imaging. *Nat Protoc* **16**, 1297–1329 (2021).

# Biophotonic composite scaffolds for controlled nitric oxide release upon NIR excitation

Sonya Ghanavati[1 2*], Evellyn Santos Magalhaes[2], Chi Nguyen[2], Bartosz Bondzior[2,3], Mika Lastusaari[4], Jeffrey Anker[5], Andrew Draganski [6,] Laeticia Petit [2], Jonathan Massera[1*]

*1. Faculty of Medicine and Health Technology, Tampere University, Korkeakoulunkatu 3, Tampere 33720, Finland*

*2. Photonics Laboratory, Tampere University, Korkeakoulunkatu 3, Tampere 33720, Finland*

*3. Institute of Low Temperature and Structure Research PAS, Okolna 2, 50-422, Wrocław, Poland*

*4. Department of Chemistry, University of Turku, FI-20014 Turku, Finland*

*5. Chemistry Department, Northwestern University, 2145 Sheridan Road, Evanston, 60208-3113, Illinois, USA*

*6. Zylö Therapeutics, Greenville, SC, USA*

## Introduction

Bone grafting is a common procedure in orthopedic, trauma, and maxillofacial surgery, aiding nearly half a million patients annually in the United States and Europe. Despite its benefits, it poses significant infection risks, often associated with biofilm formation on implants, which are resistant to antibiotics and immune responses. Bioactive glass (BAG) materials promote bone regeneration and angiogenesis due to their exceptional bioactivity and versatility. A borosilicate glass composition has recently shown promise with enhanced bioresorbability and thermal stability, enabling the fabrication of porous scaffolds suitable for targeted drug delivery and light-triggered therapeutic applications. [1, 2]

## Methods

The $26.93SiO_2$–$26.93B_2O_3$–$22.66Na_2O$–$1.72P_2O_5$–$21.77CaO$ (mol%) bioactive glass was synthesized using the melt-quenching technique, crushed to <38 µm, and mixed with $CaWO_4$ crystals codoped with $Yb^{3+}$ (15 at%) and $Er^{3+}$ (0.75 at%), prepared via solid-state reaction. Scaffolds were fabricated using the porogen burn-off method, incorporating 10 wt% crystals, with sintering at 555 °C for 1 h. S-Nitroso-N-Acetylpenicillamine (SNAP) coating facilitated NO release under 980 nm excitation, quantified using a NO analyzer, as shown in Figure 1. Scaffolds were evaluated for upconversion properties, bioactivity in simulated body fluid (SBF), mechanical strength, and cytocompatibility with human adipose stem cells (hADSCs) using Live/Dead assays and fluorescence microscopy.

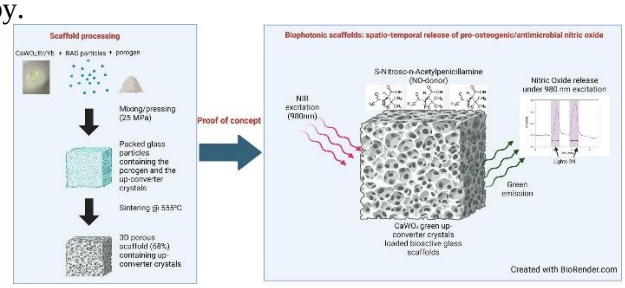


*Fig. 1: Schematic image of scaffold processing and release of Nitric oxide*

## Results

The prepared scaffolds exhibited interconnected porosity (~68%), suitable mechanical properties (compressive strength: ~1 MPa; Young's modulus: ~30 MPa), and maintained bioactivity, as indicated by hydroxyapatite formation in (SBF). Incorporation of $CaWO_4$ crystals codoped with $Yb^{3+}$ and $Er^{3+}$ enabled NIR-to-green upconversion under 980 nm excitation, with sufficient brightness (~2.23 cd/m²) to release nitric oxide (NO) from S-Nitroso-N-Acetylpenicillamine (SNAP). NO release was precisely controlled by NIR light, with no release observed in scaffolds without upconversion crystals. Cytocompatibility tests showed no adverse effects on human adipose stem cells (hADSCs), with cells remaining viable for up to 7 days in contact with the scaffolds.

## Discussion

The biophotonic scaffolds demonstrate great potential for controlled drug delivery and bone regeneration. Incorporating upconversion crystals allowed efficient NO release while maintaining scaffold integrity, bioactivity, and cytocompatibility. Consistent upconversion emissions after two weeks in SBF suggest sustained functionality, paving the way for light-triggered therapeutic systems. Future work will focus on optimizing release duration and enhancing in vivo performance.

## References

[1] Erasmus, E., P. Sule, R. Johnson, O. T. Massera, J. Sigalas, I. (2018) Sci Rep., 8(1): 3699.
[2] S. Ghanavati, L. Petit, J. Massera. (2023) J. Non-Cryst. Solids, 616: 122446.

# Impact of protein adsorption on bioactive glasses and biological response: a step forward towards a predictable cell fate

**Virginia Alessandra Gobbo (1), Andre Sanches Ribeiro (1), Enrica Vernè (2), Silvia Spriano (2), Susanna Miettinen (1), Vesa Hytönen (1), Jonathan Massera (1)**

*1. Faculty of Medicine and Health Technology, Tampere University, Finland; 2. Department of Applied Science and Technology, Polytechnic of Turin, Italy*

## Introduction

The impact of musculoskeletal diseases is increasing worldwide because of the continuous population aging. This phenomenon is negatively influencing the patients' wellbeing and graving over the societal healthcare system [1]. While a large number of biomaterials have been developed to support musculoskeletal regeneration, a strong discrepancy between *in vitro* and *in vivo* results was observed [2]. This issue was mainly attributed to a lack of understanding of the protein-material interaction, as protein adsorption is known to mediate the interactions between the implant and the surrounding environment. Protein adsorption, indeed, is a crucial phenomenon occurring at the very early stage after biomaterials implantation, determining the cell fate and, therefore, the success of the implant [3].

## Methods

Protein adsorption on bioactive glasses (BGs), a promising material class in treating musculoskeletal diseases, has been investigated. A screening on four different glass compositions, five surface modifications and three model proteins was performed. Proteins were adsorbed in static and dynamic condition, to better mimic the *in vivo* environment. Protein affinity with BGs was evaluated in terms of quantity, surface distribution and conformation, as a function of BG physicochemical properties (Fig. 1). The impact of protein adsorption on the biological response was evaluated by studying the viability, proliferation and morphology of human adipose stem cells (hASCs), and the expression of relevant osteogenic markers.

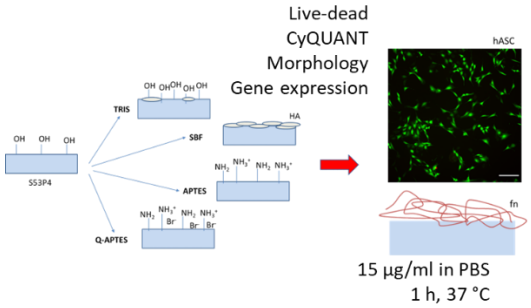


*Figure 1: Summary of the applied methods.*

## Results

Surface modification impacted on BG physicochemical properties and favoured the adhesion of selected proteins. All the surfaces showed a good cell viability, proliferation and osteogenesis. Pre-adsorbing fibronectin promoted cell alignment.

## Discussion

Controlling the surface chemistry and topography enables better prediction of the protein-material interaction as well as controlling which protein is more likely to interact with the materials' surface. The flow of the protein solution plays an important role in the dynamic protein adsorption. Fibronectin adsorption at the glass surface, prior to cell testing with hASCs, primarily affect cell orientation, indicating that proteins at the material surface highly affects the cell behavior, crucial aspect that should be taken into consideration when testing the materials *in vitro*.

## References

1. Bohara et al., Biomaterials Research, 26:26, 2022.
2. Hulsart-Billström et al., European Cells and Materials, 31:312-322, 2026.
3. Notingher et al., Mater. Charact., 49 :255-260, 2002.

## Acknowledgements

This study has received funding from the European Union's Horizon 2020 research and innovation programme under the Marie Skłodowska-Curie grant agreement No 860462 (PREMUROSA) and from Tampere University Doctoral School (Tampere, Finland).

# DRY ELECTRODE SOLUTIONS FOR MEASURING CARDIAC ACTIVITY IN WEARABLE TECHNOLOGY

**Atte Joutsen**

*Tampere University, Faculty of Medicine and Health Technology, Tampere, Finland*

## Introduction

Healthcare is under pressure due to a growing number of patients. This is because of the aging population, a sedentary lifestyle, obesity, and improved diagnosis methods. Cardiovascular diseases, including, for example, ischemic and valvular heart diseases, cardiomyopathies, and arrhythmias, are responsible for 32 percent of all deaths globally, making them the number one killer in the world. Atrial fibrillation is the most common sustained cardiac arrhythmia. In 2017, a total of 37.6 million individuals were diagnosed with atrial fibrillation and atrial flutter, a condition with a similar etiology. Atrial fibrillation can lead to complications such as ischemic stroke, heart failure, and cognitive impairment.

Wearables can offer a cost-effective alternative to traditional medical devices used in hospitals, especially in collecting long-term data on cardiac activity during free living. Electrocardiographic (ECG) recordings are traditionally made by attaching single-use wet electrodes to specific locations on the patient's body. These electrodes require preparation and are not well-suited for long-term recordings due to possible skin irritation, decreasing signal quality caused by the drying of the electrolyte, as well as the required electrode replacement at specific intervals and the loss of data in the case of lead wire disconnection.

Wearable devices with dry electrodes for ECG recordings may offer a solution to the above-mentioned challenges. Dry electrodes do not require skin preparation or electrode replacement, are well-tolerated and, when integrated into the device, correct electrode locations are ensured because of the design. The signal quality may not be as high or tolerate motion artifacts as well as wet electrodes do, but during a long-term recording, the yield of data and its quality may be sufficient for clinical decision making. This doctoral thesis aims to investigate dry electrodes to find optimal solutions for measuring cardiac activity by means of wearable technology.

## Methods

To reach the aim, a material testing study [1], three laboratory studies involving healthy participants with wearables [2-4], as well as a field study involving patients with atrial fibrillations for the purpose of validating the effectiveness of a wearable device for cardiac monitoring [5], were performed.

## Results

The findings from the studies highlight the potential of dry electrodes for measuring cardiac activity with wearable applications. Solid electrode materials, such as stainless steel and platinum, showed superior performance compared to porous materials. All dry electrode materials experienced erosion when washed repeatedly, affecting their electrical properties, but the effect was less pronounced with metallic materials. Larger electrode sizes demonstrated better performance and resilience to motion artifacts. A wrist device combining stainless steel dry electrodes with optical sensors reliably detected atrial fibrillation and was well-accepted by the users and, therefore, validated for its intended purpose.

## Discussion

The results show that solid dry electrodes of a sufficient size can be utilized to acquire long-term ambulatory ECG data of adequate quality for clinical decision making. The findings of this thesis offer novel insights into the utilization of dry electrode materials in cardiac monitoring wearables. The outcomes demonstrate the potential of the technology and can facilitate wearable device design and foster innovation in this field. Details of each study comprising this thesis are given in the references [1-5].

## References

1. Kaappa, Joutsen, et al. (2017). The electrical impedance measurements of dry electrode... DOI: 10.1108/RJTA-04-2016-0007
2. Joutsen, Kaappa, et al. (2024). ECG Signal Quality in Intermittent Long-Term Dry … DOI: 10.1038/s41598-024-56595-0
3. Kaappa, Joutsen, Vanhala (2018). Performance Analysis of Novel Flexible Electrodes for…. DOI: 10.1007/978-981-10-5122-7_60
4. Joutsen, Kaappa, et al. (2018). Dry electrode sizes in recording ECG and heart rate in… DOI:10.1007/978-981-10-5122-7_184
5. Saarinen†, Joutsen†, et al. (2023). Wrist-worn device combining PPG and ECG can be... DOI: 10.3389/fcvm.2023.1100127

# ADAPTATION OF NEAR INFRARED SPECTROSCOPY FOR IN SITU MONITORING OF TISSUE ENGINEERED CARTILAGE GROWTH

**Harini Karunarathna (1,2,3), Nithin Sadeesh (1), Omar Elkadi (1), Antti Eskelinen (4,5), Ervin Nippolainen (1), Arjen Gebraad (1,2,3), Susanna Miettinen (2,3), Isaac O. Afara (1)**

*1. Biomedical Spectroscopy Laboratory, Department of Technical Physics, University of Eastern Finland, Kuopio, Finland; 2. Adult Stem Cell Group, Faculty of Medicine and Health Technology, Tampere University, Tampere, Finland; 3. Tays Research Services, Wellbeing Services County of Pirkanmaa, Tampere University Hospital, Tampere, Finland. 4. Coxa Hospital for Joint Replacement, Tampere, Finland. 5. Faculty of Medicine and Health Technology, Tampere University. Finland.*

## Introduction

Articular cartilage lesions may remain clinically silent and unnoticed for decades [1] while morphologically progressing to osteoarthritis. As current cartilage repair procedures often fail to restore long-term physiological tissue function, tissue engineering (TE) poses an alternative for creating viable replacement tissues. However, current approaches in TE often fail to create biocompatible patient- and site-specific replacement cartilage [2] that meets the functional demands of natural joint environment. Optical spectroscopic techniques, such as near infrared spectroscopy (NIRS) can be used to evaluate connective tissue integrity to assess changes in different biomarkers during tissue growth. In this project we develop new protocols for monitoring and controlling cartilage TE using NIRS.

## Methods

We conducted cartilage TE using human bone marrow mesenchymal stem/stromal cells seeded in gellan gum and Gelatin methacrylate (GelMA) hydrogels. Constructs were cultured for up to 4 weeks in established serum-free chondrogenic differentiation medium. NIRS measurements were conducted every 24h, directly on the TE constructs using a custom setup without interfering with the TE process. Constructs were harvested at various time points (1, 3, 7, 14 and 28 days) and subjected to biomechanical testing and extensive tissue reference analysis to determine key biochemical constituents, such as glycosaminoglycans, collagen and water content, which are important biomarkers of tissue growth and development. We have assessed the relationship between the spectra and culture duration using machine learning models.

## Results

We observed that the cells seeded in gellan gum hydrogel produces more cartilage specific extracellular matrix (ECM) compared to cells seeded in GelMA. A higher cell damage in GelMA compared to gellan gum was evident. This may be due to exposure to ultraviolet light during crosslinking of GelMA, which may have affected its cell differentiation and altered production of ECM. Results of spectral data analysis show that NIRS can predict the duration of culture, indirectly linked to the quantity of matrix deposition. Hence, our preliminary analyses suggests that NIRS can accurately predict TE cartilage properties in real-time. Our machine learning analysis revealed that the top performing model was Neural Network model.

## Discussion

NIRS is a promising tool for monitoring the growth and development of engineered cartilage during TE. This optical method could be integrated into a bioreactor for *in situ* online monitoring of tissue growth during tissue engineering, potentially providing real-time information on the efficiency of the culture process. Such information could be extremely useful for optimizing and potentially personalizing the TE process. Ultimately, this study will enable development of protocols for non-destructive monitoring of the efficiency of the culture parameters, such as mechanical input, growth factors, etc. We will use our novel NIRS monitoring protocols to assess the effect of mechanical loading on tissue growth in a bioreactor.

## References

1. Palukuru, U. P., et al. Assessment of hyaline cartilage matrix composition using near infrared spectroscopy. Matrix Biol. 38, 3–11 (2014).
2. Zhou, N., et al. BMP2 induces chondrogenic differentiation, osteogenic differentiation and endochondral ossification in stem cells. Cell and tissue research, 366, 101-111. (2016).

# DECIPHERING CEREBELLAR ASTROGLIAL CALCIUM DYNAMICS WITH DETAILED WHOLE-CELL MODELING

**Laura Keto (1), Tiina Manninen (1)**

*1. Faculty of Medicine and Health Technology, Tampere University, Finland*

## Introduction

Astroglial cells partake in cerebellar information processing via hundreds of nanoscopic processes that give rise to a diverse array of spatiotemporally complex calcium signaling. We present here a Blender-based toolkit CellRemorph [1] to address the specific challenges and requirements of building detailed astrocyte models that capture their complex and functionally relevant nanoscale architecture. We applied the CellRemorph toolkit for building a whole-cell model of a cerebellar astroglial cell to study how its calcium dynamics are influenced by its detailed nanogeometry.

## Methods

The CellRemorph toolkit is freely available at GitHub (https://github.com/lauraketo/CellRemorph) and includes tools for transforming, selecting and slicing astroglial cell structures. We utilized the CellRemorph tools alongside NEURON [2] and ASTRO [3] to construct a detailed model of a cerebellar astroglial cell (Fig. 1). The model featured a stem tree [4] populated with nanoscopic processes [5] enabling us to analyze calcium signaling patterns throughout the entire cell morphology.

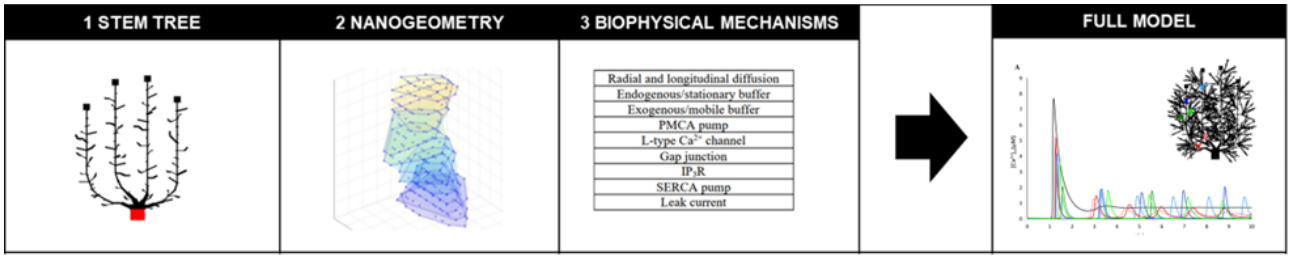


*Figure 1: The cerebellar astroglial cell model was composed of three components (stem tree, nanogeometry, and biophysical mechanisms). The full model was utilized for simulating calcium dynamics across the whole morphology.*

## Results

The spatiotemporal pattern of calcium wave dynamics across the cerebellar astroglial morphology was influenced by the shape and localization of the lateral processes. Through simulations conducted both with and without calcium buffers, we were able to study how the unique nanogeometry of these cells impact their calcium signaling and elucidate the highly variable spatiotemporal calcium dynamics that occur within the specialized morphological structures of cerebellar astroglial cells.

## Discussion

The path from experimental data into morphologically detailed simulations requires novel methods to accommodate complex cell morphologies. The CellRemorph toolkit includes three new tools that facilitate the creation of realistic astrocyte cell models for different types of morphologically detailed simulations. In this work, for the first time a whole cerebellar astroglial cell was modeled in the detail of nanoscopic processes. The utility of the CellRemorph tools extends beyond astroglial cells, and the toolkit may prove useful for constructing detailed models for other computationally less studied brain cell types, such as microglia and oligodendrocytes, as well.

## References

1. Keto & Manninen, Neuroinformatics, 21: 483–500, 2023.
2. Carnevale & Hines, Cambridge University Press, 2006.
3. Savtchenko et al., Nat Commun, 9: 3554, 2018.
4. Lippman et al, Glia, 56(13): 1463–1477, 2008.
5. Grosche et al, Nat Neurosci, 2(2): 139–143, 1999.

## Acknowledgements

We are very grateful to Prof. Helmut Kettenmann for providing us cerebellar astroglial morphological data. The work was supported by the Research Council of Finland (Nos. 326494, 326495, 345280, 355256).

# ESTIMATING KNEE JOINT CARTILAGE MECHANICS USING FINITE ELEMENT BY NEURAL NETWORK BASED KINETIC DATA

**Mahan Nematollahi (1), Amir Esrafilian (1), Jere Lavikainen (1), Mika E. Mononen (1), David J. Saxby (2), David G. Lloyd (2), Rami K. Korhonen (1)**

*1. University of Eastern Finland, Kuopio, Finland; 2 Griffith University, Queensland, Australia*
*Email: Mahan.nematollahi@uef.fi*

## Introduction

We developed our previous method to investigate knee cartilage stresses and strains using a finite element (FE) model assisted by artificial intelligence (AI)-based kinetic data. The data was obtained from artificial neural networks (ANNs) with specific information of the study participants. For comparison, a FE model driven by 3D motion capture (Mocap) and musculoskeletal modeling (MSM) was generated. Results showed maximum principal stresses in the medial tibial cartilage were similar between the modeling approaches. Low-fidelity, AI-assisted approaches are increasingly used to estimate human musculoskeletal kinematics and kinetics traditionally measured by high-fidelity, Mocap-assisted approaches [1]. Less attention has been given to tissue mechanics (i.e., stress and strain) estimated with low-fidelity methods, which are crucial developments for out-of-lab estimation of tissue degeneration or failure. Herein, we estimated knee joint cartilage mechanics during gait using FE models driven by 3D Mocap- and AI-assisted data.

## Methods

Healthy participants (4 females, 5 males; age 30±7 years; body mass index 27±7 kg/m²) were studied. Marker trajectories and ground reaction forces were recorded during walking gait in a Mocap laboratory, and magnetic resonance imaging was used to generate knee geometries. For the high-fidelity approach, Mocap data were used in OpenSim and CEINMS to estimate knee joint contact forces, moments, and flexion angle (Fig. 1A) and used as inputs in the high-fidelity FE models that included cartilage, menisci, and ligaments (Fig. 1B) [4]. For the low-fidelity approach, ANNs were used to estimate knee joint contact forces from the subjects' information (Fig. 1A) [2,3] and, with a generic flexion angle, used as inputs in the low-fidelity FE models that consisted of cartilages, with the effects of menisci and ligaments considered in the boundary conditions (Fig. 1B). FE meshes for the models were generated using auto-segmentation [4]. Maximum principal stresses during the stance phase were analyzed (see Fig. 1C for one person).

## Results and Discussion

In the medial tibial cartilage, average stress values were not significantly different between the modeling approaches ($P>0.05$, Fig. 1D). The only significant differences in the peak stresses were observed in the lateral tibial cartilage at ~80% of stance ($P<0.05$). Further model refinements are needed to improve the predictive accuracy in the lateral tibial cartilage. We present a method to estimate knee joint cartilage mechanics during gait without marker-based Mocap. This approach will enable out-of-lab tissue failure estimation, degeneration prediction, as well as rehabilitation planning and self-management of musculoskeletal diseases.

## References

[1] Song *et al.* (2023) *J Biomech*, **157:** 111751
[2] Paz *et al.* (2024) *Ann Biomed Eng.*, **52**: 2569-83
[3] Lavikainen *et al.* (2023) *Ann. Biomed. Eng.*, **51**: 2479–89
[4] Esrafilian *et al.* (2025) *IEEE Trans Biomed Eng.*, **72**: 56-69

## Acknowledgements

Sigrid Jusélius Foundation, Research Council of Finland, Marie Skłodowska-Curie GA# 101108335, NHMRC 2001734 in Australia.

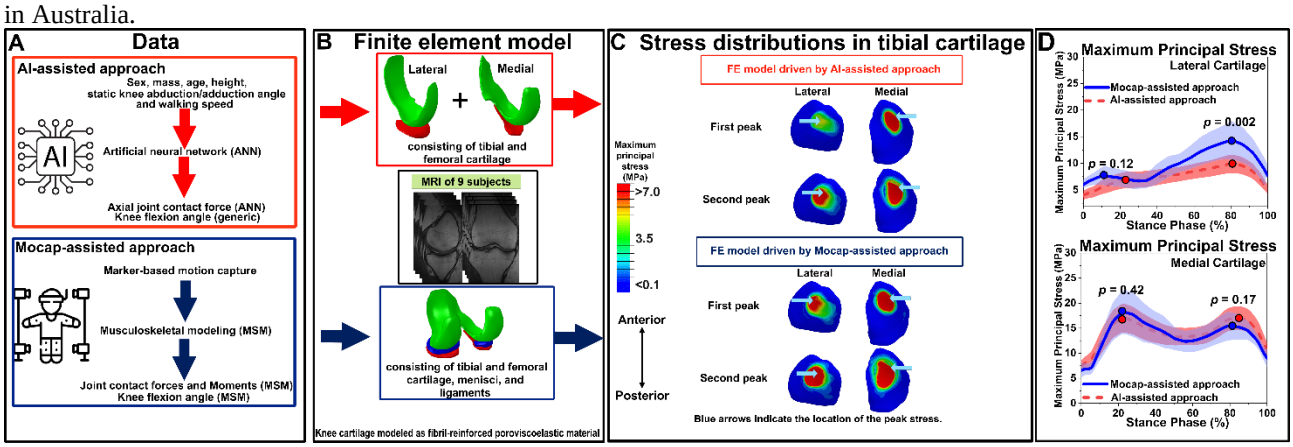


*Figure 1: Workflow and results of the finite element models driven by Mocap- and AI-assisted approaches.*

# INVESTIGATING EFFECTS OF INFLAMMATION ON JOINT TISSUES VIA NEAR-INFRARED (NIR) SPECTROSCOPY ON EXPLANT CULTURE

**Nithin Sadeesh[1], Fatemeh Safari [2], Zhen Li[2], Arjen Gebraad[1,3,4], Ervin Nippolainen[1], Susanna Miettinen[3,4], Sybille Grad[2], Isaac O. Afara[1]**

*[1] University of Eastern Finland, Finland, [2]AO Research Institute, Switzerland; [3], Tampere University, Finland., [4] Tampere University Hospital, Finland.*

## Introduction

Chronic joint disorders, like osteoarthritis (OA) are characterized by local inflammation and complex interactions within joints (1). Despite significant progresses, many aspects of their pathophysiology remain unclear (2), and the role of inflammatory biomarkers is not fully understood due to unreliable models and real-time detection methods (3). Traditional methods like ELISA and mass spectrometry for assessing glycosaminoglycans (GAG) and nitric oxide (NO) release are accurate but costly and time-consuming (4,5). We aim to address these issues using near-infrared spectroscopy (NIRS) combined with machine learning (ML) for rapid, non-destructive assessment of GAG and NO release (6,7).

## Methods

Bovine osteochondral explants and synovium (n=24) were co-cultured in DMEM high glucose (HG) and low glucose (LG) media, supplemented with antibiotics, ITS + Premix, non-essential amino acids, and ascorbic acid, with or without inflammatory factors (IF) TNF and IL1B. GAG and NO release were measured daily over 14 days (336 samples) using dimethyl-methylene blue and Griess assay, respectively. NIR spectral data were acquired in transflection mode using a fiber optic probe (Figure 1a) (6) and StellarNet-spectrometer (900-1700nm) and analyzed with the QUASAR-Orange tool. ML algorithms (Adaptive Boosting (AdaBoost), and Support Vector Machine (SVM)) classified the spectral data into four classes based on medium composition.

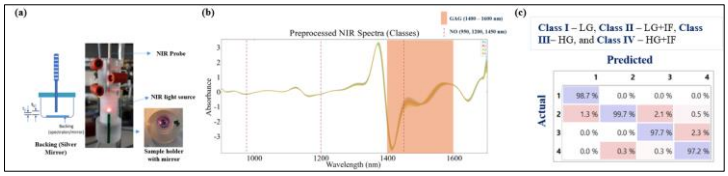


***Figure 1: (a) Custom experimental setup** for NIR spectroscopic assessment of tissue culture media**. (b) NIR spectra changes** for GAG were correlated to the 1400-1600 nm range, while NO levels were associated with peaks at 950, 1200, and 1450 nm. **(c) Confusion matrices of ML models** show that the SVM model was the best-performing one.*

***Table 1 - Classification performance metrics for NIR spectra of medium samples across four classes***

| Model | AUC | CA | F1 | Prec | Recall | MCC |
|---|---|---|---|---|---|---|
| **SVM** | 0.999 | 0.983 | 0.983 | 0.984 | 0.983 | 0.978 |
| **AdaBoost** | 0.936 | 0.904 | 0.904 | 0.904 | 0.904 | 0.872 |

## Results

GAG and NO production were significantly influenced by glucose concentration and inflammatory factors. HG and IF produced the highest GAG levels, with IFs increasing GAG and NO levels in both glucose conditions. Preliminary results show that NIRS combined with ML algorithms, specifically SVM and AdaBoost models, can effectively classify culture media based on composition, enabling precise monitoring of GAG and NO levels under varying conditions (Figure-1b, Table-1).

## Discussion

We demonstrated the potential of NIRS for assessing the influence of inflammatory factors on biomarker release in culture media. Preliminary results show NIRS can rapidly detect low concentrations of GAG and NO in biofluids, offering insight into changes in media composition. Ongoing studies aim to quantify GAG and NO concentrations using NIRS.

## References

(1) Mazur, C. M., et al (2021), *AAOS*. (2) Watt FE., et al (2023). Curr Opin Rheumatol. (3) Salman, L. A.,et al (2023). *Arthritis Research and Therapy*. (4) Ossendorff, R., et al (2024). *International Journal of Molecular Sciences*. (5) Fernández-Metzler, C., et al (2022). *The AAPS Journal*. (6) Sadeesh, N, et al (2025). Unpublished. (7) Afara, I. O., et al (2021). *Nature Protocols.*

# IMPAIRED MEMORY STORAGE AND RECALL OF HIPPOCAMPAL CA1-CA3 NETWORK IN EARLY ALZHEIMER'S DISEASE

**Saana Seppälä (1), Fabio Librizzi (2), Marja-Leena Linne (1), Justinas J. Dainauskas (3,4), Hélène Marie (5), Michele Migliore (2), Ausra Saudargiene (3,4)**

*1. Faculty of Medicine and Health Technology, Tampere University, Tampere, Finland; 2. Institute of Biophysics, National Research Council, Palermo, Italy; 3. Neuroscience Institute, Lithuanian University of Health Sciences, Kaunas, Lithuania; 4. Department of Informatics, Vytautas Magnus University, Kaunas, Lithuania; 5. Institut de pharmacologie moléculaire et cellulaire, CNRS, INSERM, Université Côte d'Azur, Valbonne, France*

## Introduction

Memory storage and recall are fundamental processes of the hippocampus, adversely affected by neurodegenerative diseases like Alzheimer's disease (AD). While the exact molecular mechanisms behind AD are not fully understood, the dynamics between synaptic plasticity dysfunction and neuronal loss remains a key area of study. For example, accumulation of Amyloid-β peptide (Aβ), due to alterations in the processing and clearance of the amyloid precursor protein, is agreed to play a role in the neurodegeneration. Being able to bind to the N-methyl-D-aspartate receptors (NMDARs), excess Aβ can lead to over-activation of these receptors. This can result in abnormal neuronal activity (1,2) and eventually impaired synaptic plasticity and long-term potentiation (LTP) (3). However, recent research has shown that the impaired LTP can be restored with a pharmacological blockage of a specific NMDAR subunit, GluN2B-NMDAR. These effects have been studied at the cellular level (see, e.g. 4), but it remains important to explore how they influence larger populations of neurons at the network level.

## Methods

Here, we present a phenomenological computational model, combining previously published network model of 100 hippocampal CA1 pyramidal neurons (5) and a NMDAR-dependent synaptic plasticity model (4). To present evidence of the adverse effect of AD to the memory encoding at a network level, we performed simulations for conditions describing control (healthy), accumulation of Aβ and recovery of the synapses due to an inhibition of the GluN2B-NMDAR subunit. All simulations were performed with NEURON model builder (version 8.2.4).

## Results

We successfully translated the previously studied cell-level observations of memory encoding to describe these phenomena at a network level. Our results indicate that also at a network level, the increased Aβ concentration impairs the LTP function at hippocampal CA1-CA3 synapses, leading to weakening of the affected connections. We also show that suppressing the activity of the GluN2B-NMDAR subunit restores the LTP function with respect to the control.

## Discussion

Our model integrates molecular, cellular and network-level interactions at a systems level perspective of Alzheimer's disease. By linking cell-level events to a higher scale network dysfunction, our findings offer insights into memory impairments at a higher cognitive level, advancing the study of neurodegeneration. Alzheimer's disease poses significant health and socio-economic challenges, which drive its scientific impact. A deeper understanding of its pathology is essential for developing effective strategies to mitigate its widespread consequences.

## References

1. Peng et al., Molecular Psychiatry, 27(7):2940–2949, 2022.
2. Wang & Reddy, Journal of Alzheimer's Disease, 57(4):1041–1048, 2017.
3. Walsh et al., Nature, 416(6880):535–539, 2002.
4. Dainauskas et al., Frontiers in Computational Neuroscience, 17, 2023.
5. Bianchi et al., Hippocampus, 24(2):165–177, 2014.

## Acknowledgements

Research Council of Lithuania, Agence Nationale de la Recherche (Flagship ERA-NET Joint Transnational Call JTC 2019 with Human Brain Project, No. S-FLAG-ERA-20-1/2020-PRO-28), Horizon Europe (Specific Grant Agreement No. 101147319, EBRAINS 2.0), Swiss National Supercomputing Centre (CSCS) under project ID ich002; Italian National Recovery and Resilience Plan (NRRP), M4C2, funded by NextGenerationEU (Project IR0000011, CUP B51E22000150006, EBRAINS-Italy)

# COMBINING MICROFLUIDIC TECHNOLOGY WITH HUMAN BASED CELL MODELS TO BUILD BODY-ON-CHIP FOR STROKE-HEART SYNDROME

**Kaisa Tornberg[1], Saara Haikka[1], Emma Pesu[2], Elias Kuusela[2], Anna-Mari Moilanen[3], Emre Kapucu[3], Mila Huovinen[1], Kardelen Yilmaz[1], Satu Jäntti [3], Henna Lappi[2], Mari Pekkanen-Mattila[2], Oommen P. Oommen[4], Katriina Aalto-Setälä[2], Susanna Narkilahti[3], Pasi Kallio[1]**

*1 Micro- and Nanosystems Research Group, Faculty of Medicine and Health Technology, Tampere University, Tampere, Finland*

*2 Heart Group, Faculty of Medicine and Health Technology, Tampere University, Tampere, Finland*

*3 Neuro Group, Faculty of Medicine and Health Technology, Tampere University, Tampere, Finland*

*4 School of Pharmacy and Pharmaceutical Sciences, Cardiff University, UK*

## Introduction

Organ-on-a-chip technology combines microfluidic devices with living organ subcultures to model human organs and their functions within the laboratory settings. In my PhD thesis, I develop microfluidic devices to study interaction between human brain and heart. More specifically, I develop technology to model Stroke-Heart syndrome where we emulate the interaction between the brain facing stroke and the human heart. The developed microfluidic device contains coculture structures to implement different cell types within their own compartments to resemble brain and peripheral neurons connecting to the heart. The cells are connected via microtunnels, and the oxygen environments are controlled with gas flowing in microchannels positioned beneath the compartments. To model the oxygen depletion that the brain faces during stroke, the oxygen environment needs to be controlled precisely.

## Methods

Chips are fabricated utilizing soft lithography using polydimethylsiloxane (PDMS) as the fabrication material. We have established a ratiometric oxygen sensing setup to characterize the microfluidic devices and their oxygen modulation dynamics. [1] Devices were first proven to be suitable for cell culture using a commercially available Live/Dead cell staining kit and later on optimized for the cell types representing brain, peripheral neurons and the heart, all derived from human induced pluripotent stem cells (hiPSC). Image-iT™ Green Hypoxia Reagent was used to study if the cells within the brain compartment respond to the decreased oxygen tension.

## Results

The structure is capable of decreasing the oxygen tension within minutes. Measurements show that different oxygen profiles can be created simultaneously to different compartments, while cells stay connected via the microtunnels. As live/dead staining showed the structure being suitable for cell culture, we accommodated the structure successfully to relevant cell types to establish compartments for the brain, peripheral neurons and heart. The compartment resembling brain was exposed to decreased oxygen tension and cells respond accordingly.

## Discussion

We successfully multicultured human derived cells in the microfludic device to resemble brain, peripheral neurons and heart. We were also able to show that oxygen tension can be decreased in one of the compartments in time scale that is relevant for stroke and thus this platform can be used to study the interactions taking place in Stroke-heart syndrome.

## References

1. Tornberg, K., Biomedical Microdevices 24, 2022. doi:10.1007/s10544-022-00634-y

## Acknowledgements

This work was supported by Research Council of Finland, for the funding (Centre of Excellence in Body-On-Chip Research grant number 353174, 353175 and 353176). In addition Kaisa Tornberg would like to acknowledge the support from Finnish Cultural Foundation, the Pirkanmaa Regional Fund and doctoral school of Faculty of Medicine and Health Technology, Tampere University.

# MULTIVARIATE DIRECTED FUNCTIONAL CONNECTIVITY METHODS FOR ESTIMATION OF WHOLE-BRAIN CONNECTIVITY

**Katja Törmä, Jari Hyttinen, Narayan Puthanmadam Subramaniyam**

*1. Faculty of Medicine and Health Technology, Tampere University, 33520 Tampere, Finland*

## Introduction

Understanding how connections between brain regions transfer information and how such connections change (e.g., due to a neurological disorder) is a major goal in neuroscience [1]. To address this, various functional connectivity measures have been developed [1]. This study aims to evaluate the performance of three different connectivity measures using simulated (EEG) signals and comparing the resulting connectivity maps to the known ground truth.

## Methods

Three multivariate functional connectivity methods: partial directed coherence (PDC), multivariate transfer entropy (mTE) and PCMCI. These methods were applied on simulated EEG signals, produced with Jansen-Rit neural mass model with known connectivity between the signals. Four parameters were studied: the number of nodes, connection density, sample size as well as the signal-to-noise ratio (SNR). The performance of these methods was evaluated by calculation of the F1-score.

## Results

mTE performed the best regardless of the parameter changes, giving the highest F1-score (Figure 1). Increasing the network size reduced the F1-scores for all connectivity measures. PDC was the most sensitive to noise, with its F1-score dropping from 0.9 to 0 as the SNR decreased. In contrast, PCMCI and mTE were more robust to noise, maintaining F1-scores between 0.6 and 1. A similar trend was observed for sample size: PDC's performance dropped considerably as sample size decreased, while PCMCI and mTE maintained more consistent F1-scores.

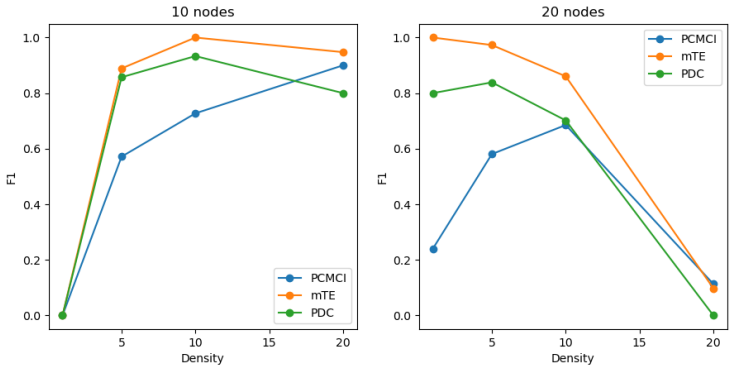


*Figure 1: Comparison of three connectivity measures. The figures show the effect of change in connectivity strength in terms of F1-score for two different sized networks (10 nodes, 20 nodes).*

## Discussion

In conclusion, mTE outperformed the other two methods in all cases. Between PCMCI and PDC, PCMCI produced more stable results for changes in parameters. However, despite the good performance of mTE, it requires the most computation time, which is a very limiting factor in using mTE for the analysis of whole-brain connectivity involving hundreds of regions. Thus, it would be useful to further investigate and improve connectivity measures to obtain performance similar to mTE but with lower computational demands.

## References

1. Chiarion, G. et al. Bioengineering 10, (2023)

## Acknowledgements

This work was supported by the Finnish Ministry of Education and Culture's Pilot for Doctoral Programmes (Pilot project for Mathematics of Sensing, Imaging and Modelling)